Strong Winds of Magnetic Massive Stars

Asif ud-Doula
Penn State Scranton

PennState
Scranton

Introduction

- Line-driven winds
- Magnetism in stars
- Numerical simulations/models
- Results, implications

Main Sequence Stars

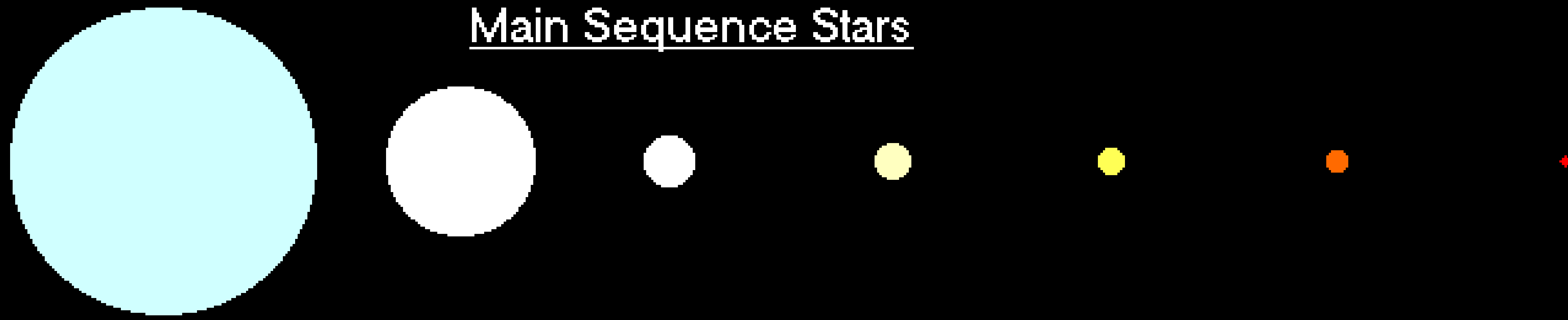

Spectral Type:	O	B	A	F	G	K	M
Temperature:	40 000K	20 000K	8500K	6500K	5700K	4500K	3200K
Radius (Sun=1):	10	5	1.7	1.3	1.0	0.8	0.3
Mass (Sun=1):	50	10	2.0	1.5	1.0	0.7	0.2
Luminosity (Sun=1):	100 000	1000	20	4	1.0	0.2	0.01
Lifetime (million yrs):	10	100	1000	5000	10 000	50 000	100 000
Abundance:	0.00001%	0.05%	0.3%	1.5%	4%	9%	80%

Giant Stars

Low mass stars near the end of their life.

Spectral Type:	G, K or M
Temperature:	4000K
Radius (Sun=1):	20
Mass (Sun=1):	1.2
Luminosity (Sun=1):	200
Lifetime (million yrs):	10
Abundance:	0.5%

White Dwarfs

Dying remnant of an imploded star.

Spectral Type:	D
Temperature:	Under 50 000K
Radius (Sun=1):	Under 0.01
Mass (Sun=1):	Under 1.4
Luminosity (Sun=1):	Under 0.01
Lifetime (million yrs):	–
Abundance:	5%

Supergiant Stars

High mass stars near the end of their life.

Spectral Type:	B, A, F, G, K or M
Temperature:	4000 to 40 000K
Radius (Sun=1):	30 to 500
Mass (Sun=1):	10 to 70
Luminosity (Sun=1):	30 000 to 1000 000
Lifetime (million yrs):	10
Abundance:	0.0001%

r powell

Mass Loss from Stars

- Stars like the sun lose very little mass ~10^{-14} MSun/yr
- Solar wind is driven by gas pressure gradient
- Hot/massive stars (O and B type) lose 10^{-9}~10^{-5} MSun/yr
- Hot star winds are driven by scattering of radiation by resonance lines of heavy ions.

Sound speed; thermal pressure has little significance.

Light's Momentum

- Light has momentum, $p=E/c$
- Usually neglected, because c is so high
- But becomes significant for very bright stars
- Key question: how big is this force vs. gravity?

Light As a Driving Mechanism

- Free Electron (continuum) Scattering
- Bound Electron (line) Scattering
  - Can be much stronger than free electron scattering

Light As a Driving Mechanism

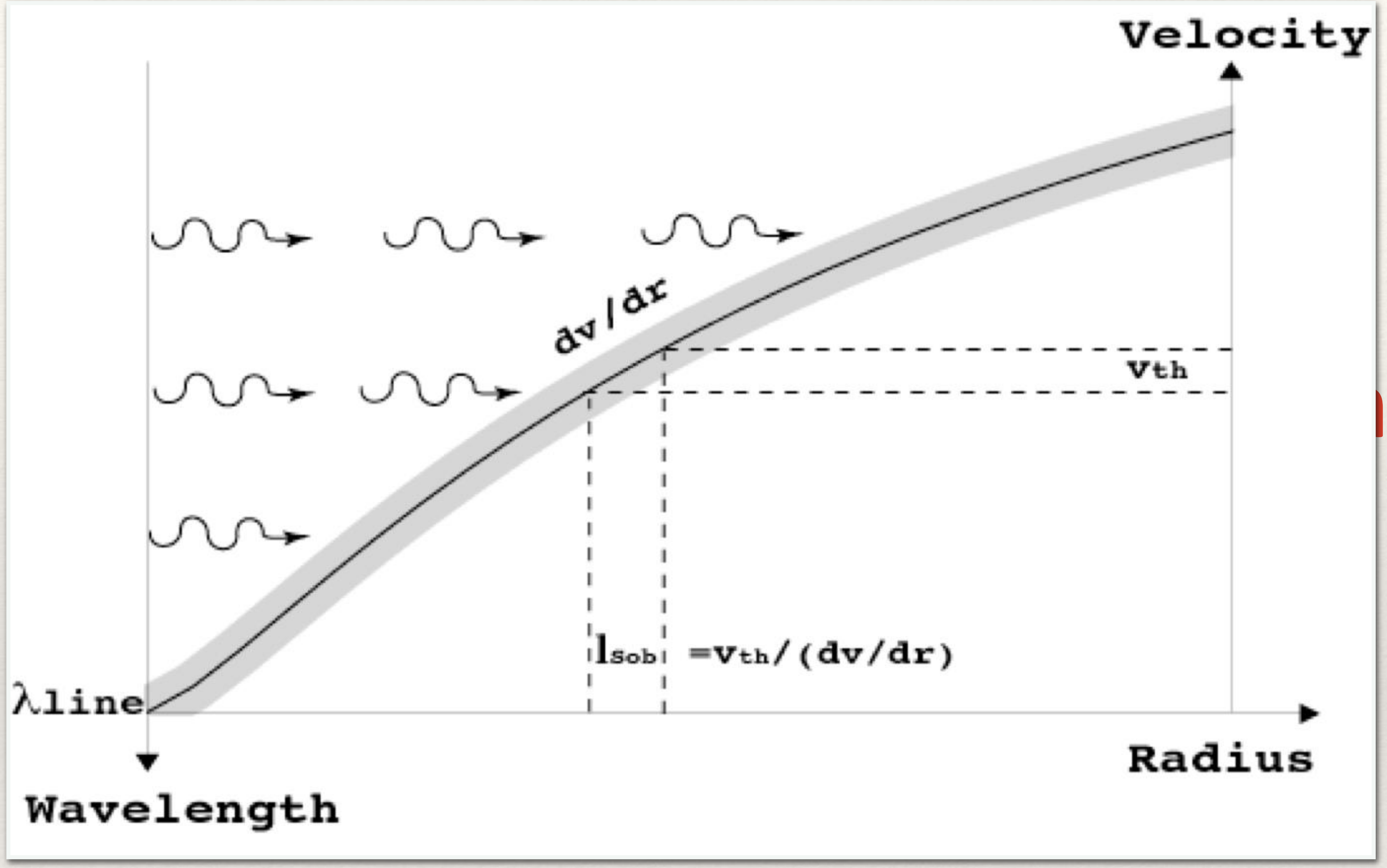

$L_{sob} << R_*$

For strong,

optically thick lines

$$g_{thick} \sim \frac{g_{thin}}{\tau} \sim \frac{1}{\rho}\frac{dv}{dr}\tau \equiv \kappa\rho\,\frac{v_{th}}{dv/dr}$$

Line Force From an Ensemble of Lines in CAK theory

If we take into account all available thick and thin lines, the line force is:

$$g_{lines} \approx \overline{Q}\,\frac{\kappa_e L}{4\pi r^2 c}\left(\frac{dv/dr}{\rho c \overline{Q}\,\kappa_e}\right)^{\alpha}$$

Free e- scattering

1D CAK Model of ZPup

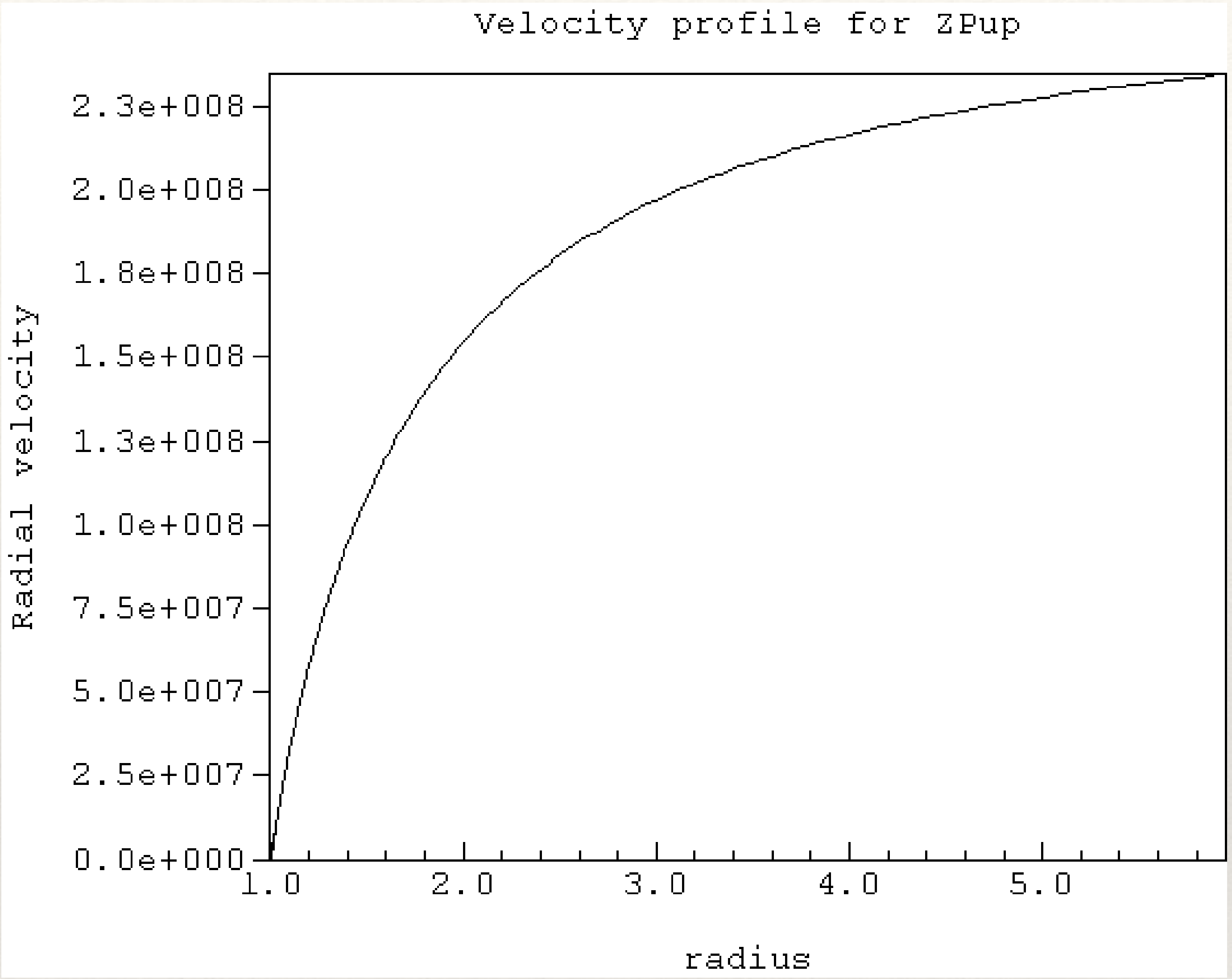

Steady & spherically symmetric

well characterized by

$$v(r) = v_\infty (1 - R_* / r)^\beta$$

Observational evidence:

unsteady, spherically non-symmetric.

Discrete Absorption Features

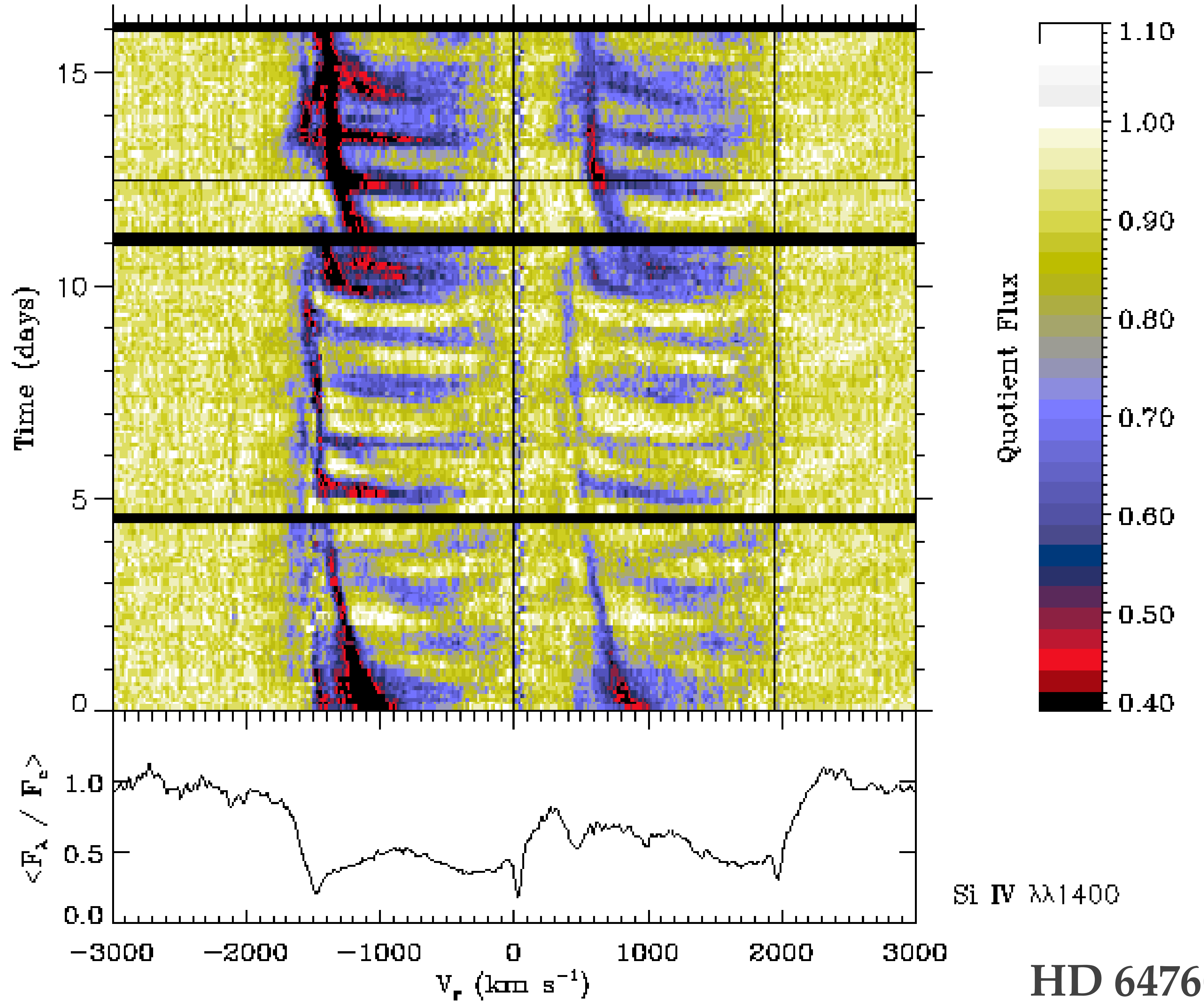

HD 64760 (B Star)

Magnetic Effects on Solar Coronal Expansion

1991 Solar Eclipse

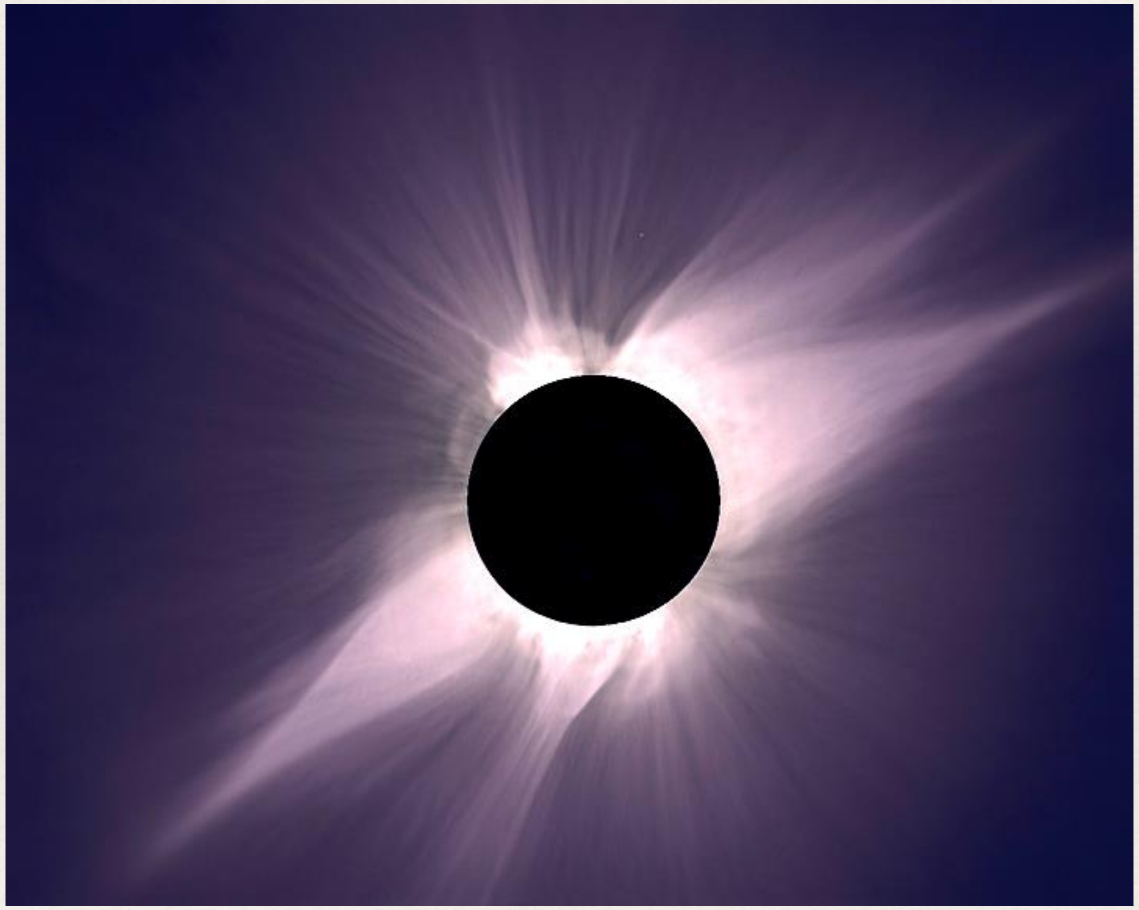

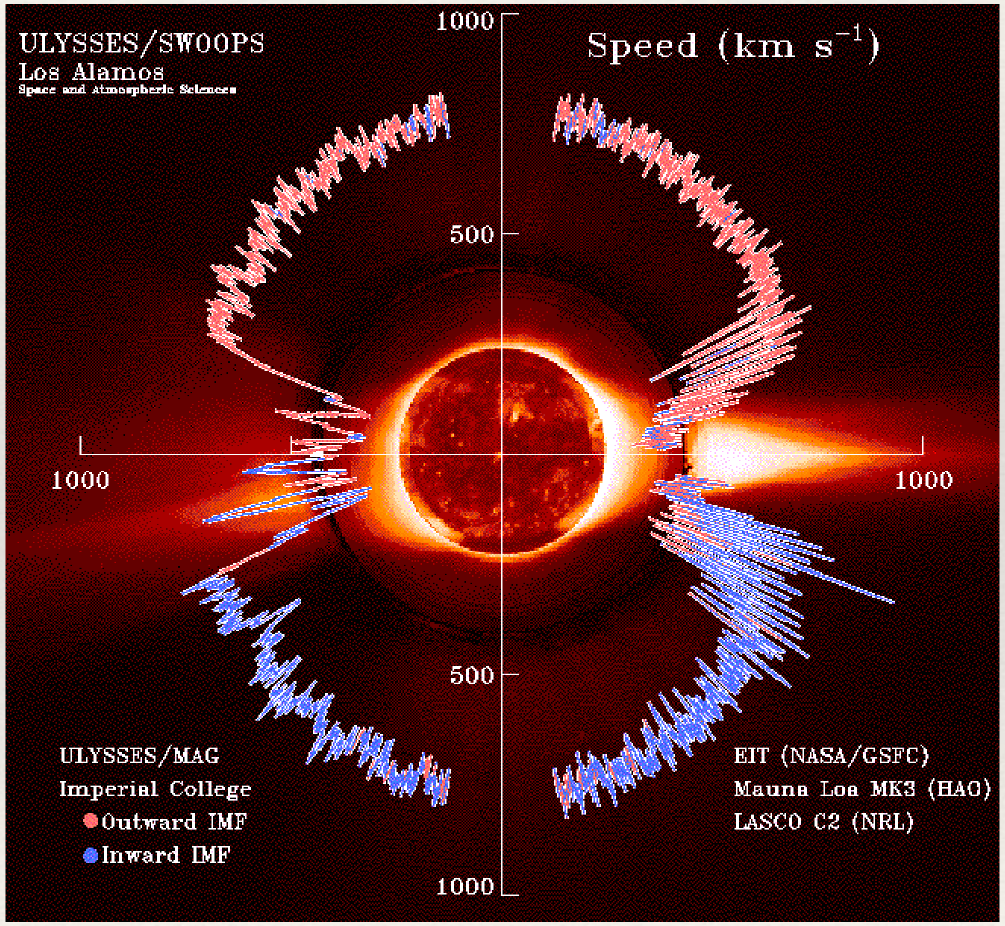

Where do we find stellar magnetism ?

The Hertzsprung-Russell diagram of stars

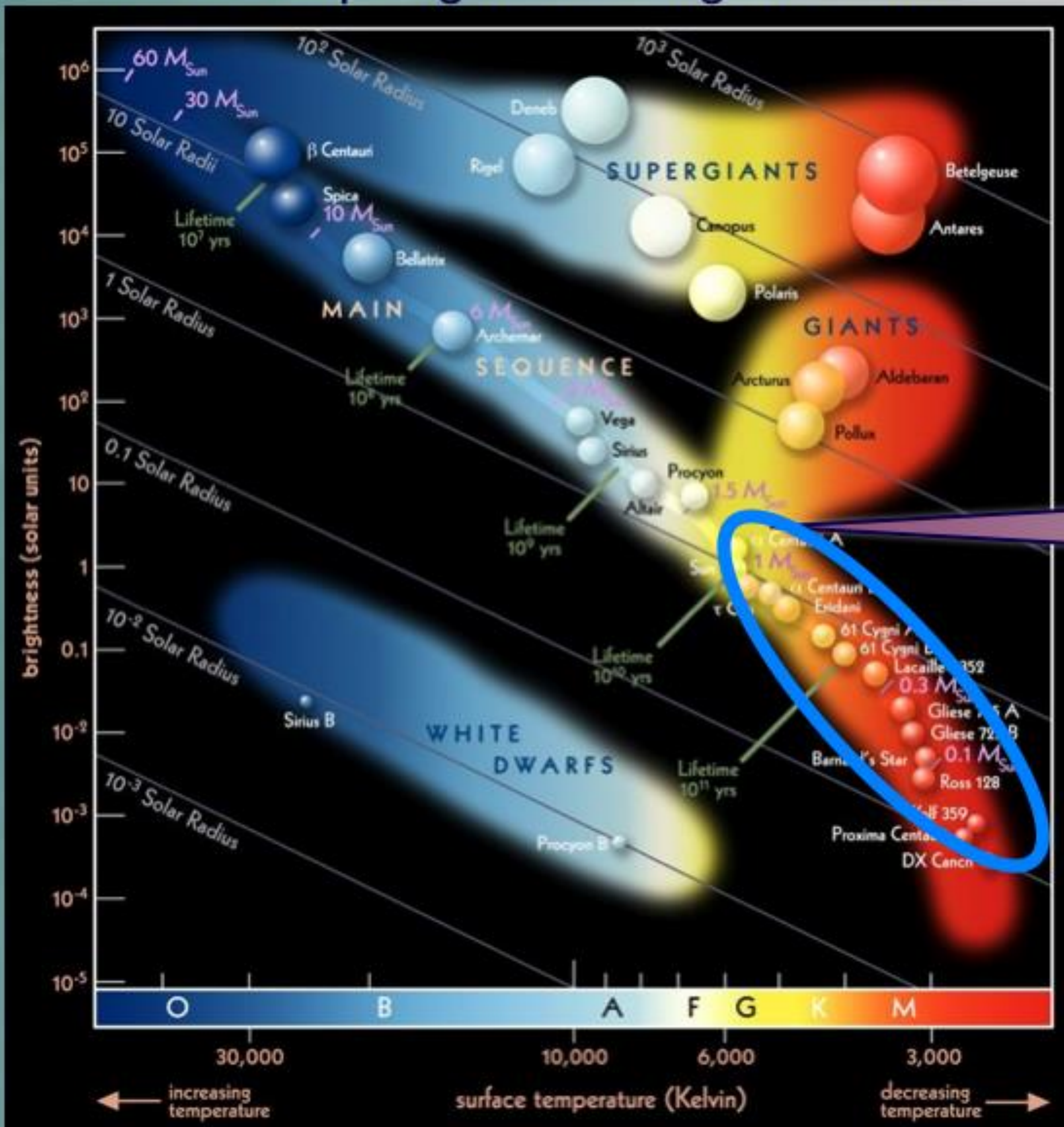

Our Sun

1 kGauss = 0.1 Tesla

Courtesy: V. Petit

The Sun and its fellow low-mass stars

<u>Cool stars with convective envelopes</u>

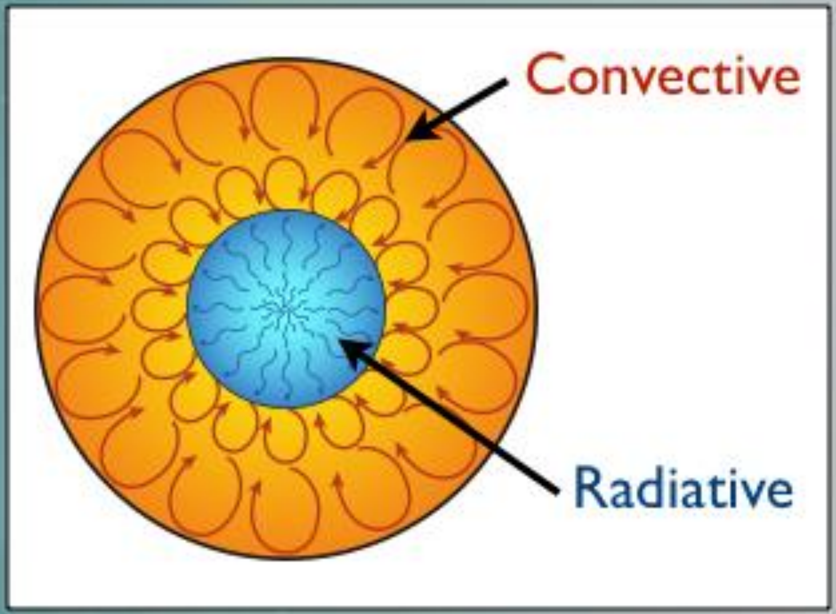

Topologically complex

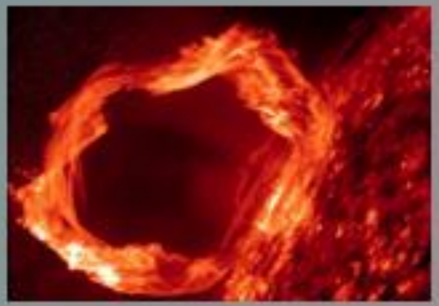

Dynamic on various timescales (hh, dd, yy)

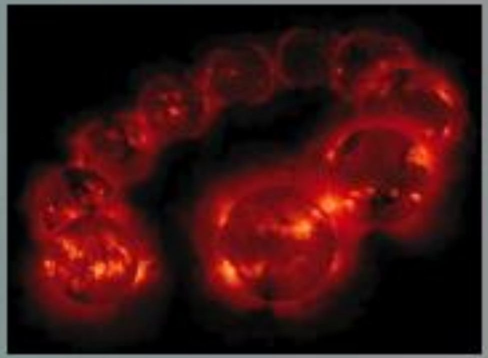

Courtesy: V. Petit

Where do we find stellar magnetism ?

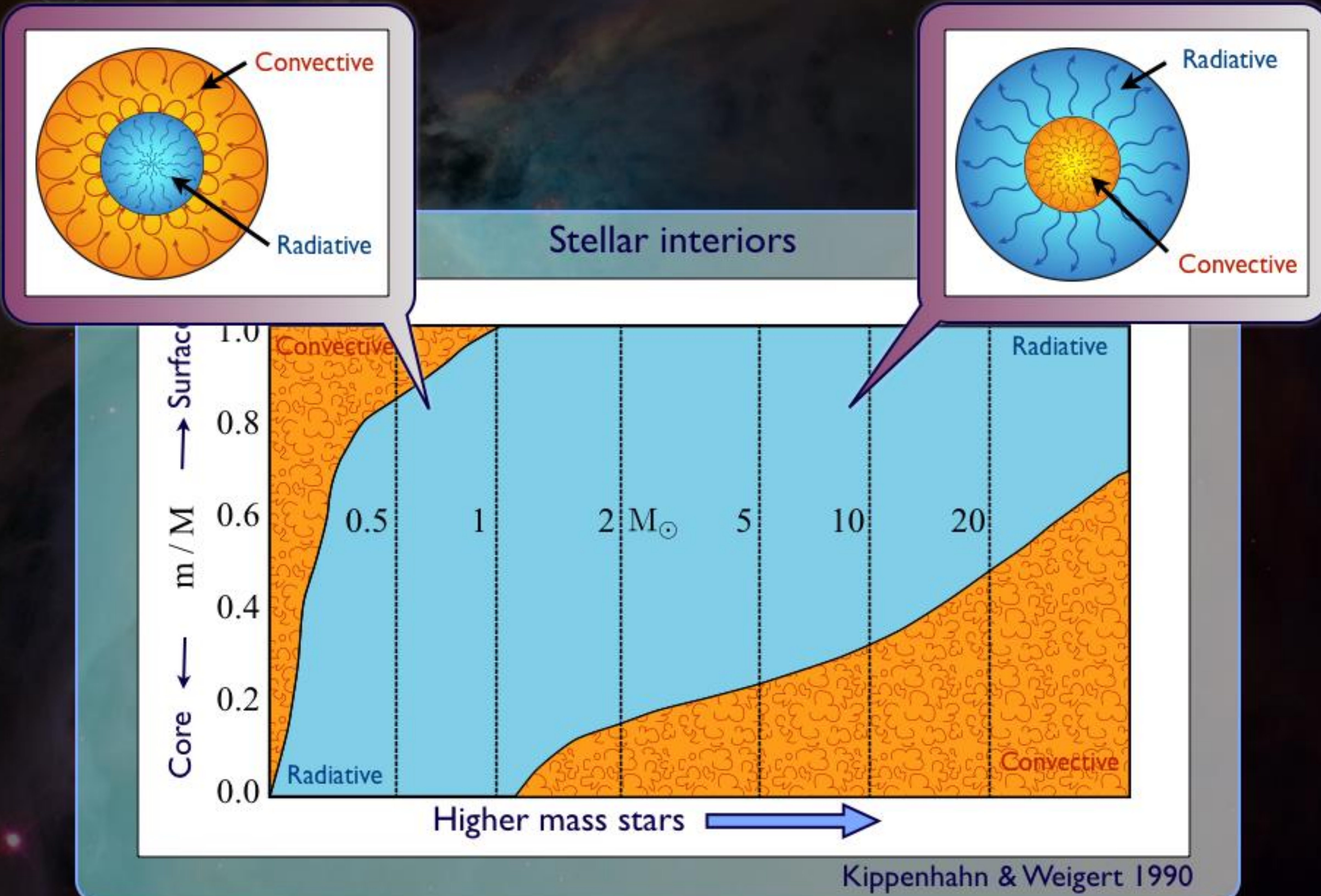

Kippenhahn & Weigert 1990

Chemically Peculiar Magnetic ApBp Stars

Volume limited (100pc) sample of A- and late-B stars

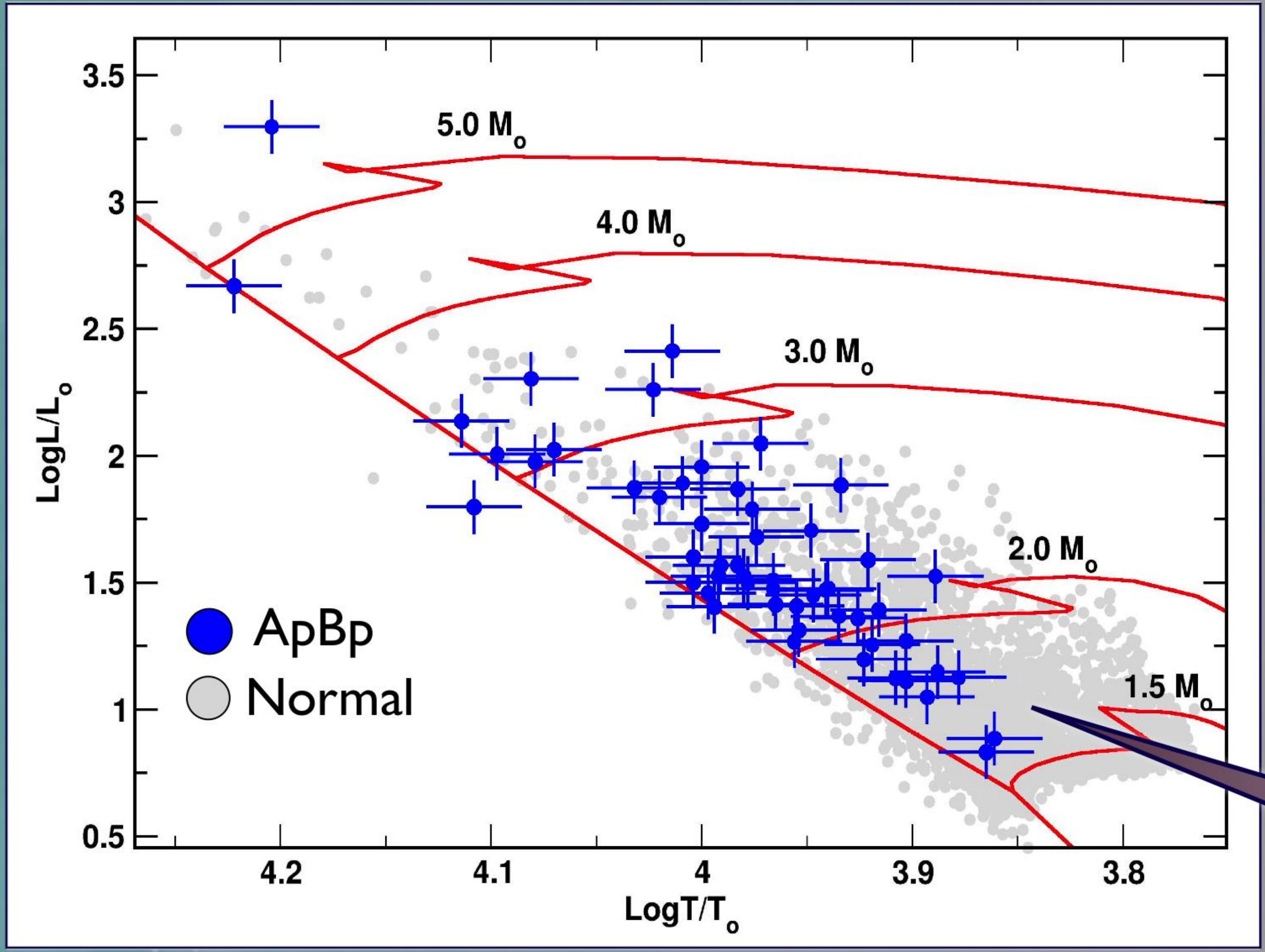

Power et al. (2007)

- Strong (kG)
- Large-scale

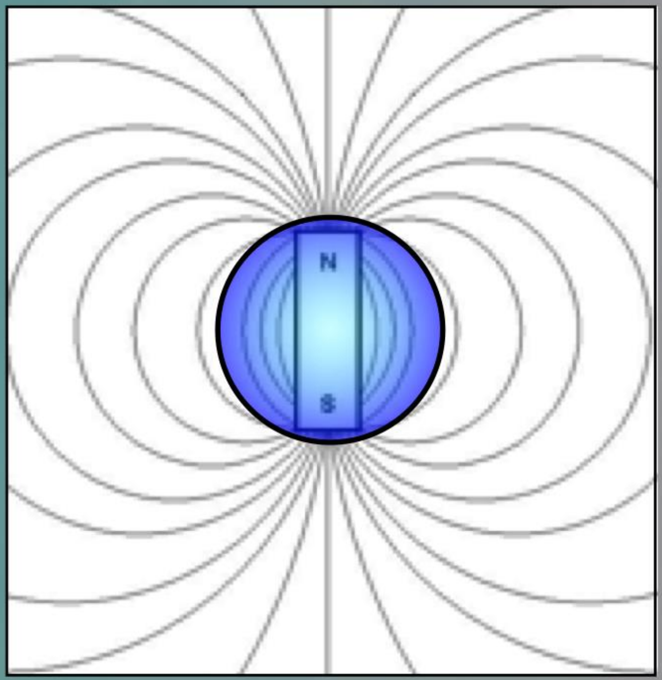

Incidence: 10%

About 10% of massive stars are magnetic.

Grunhut+2017

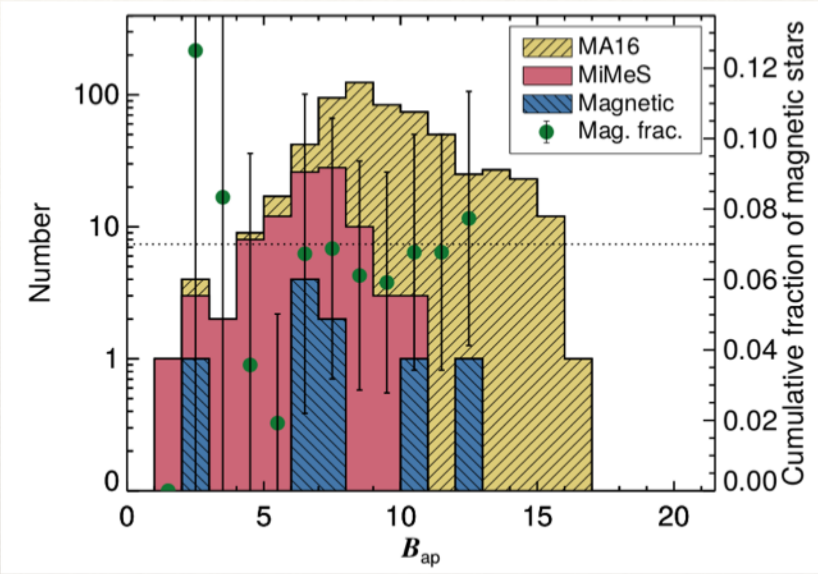

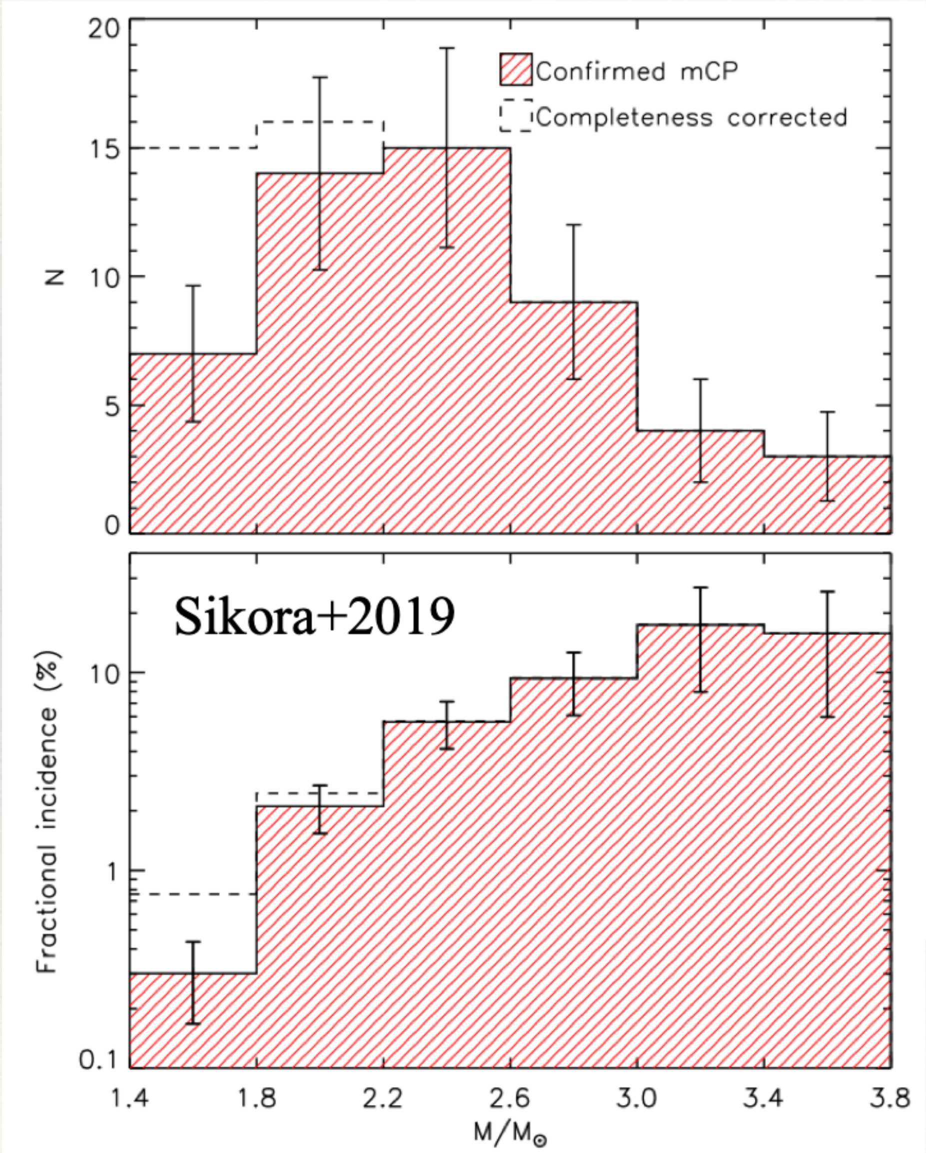

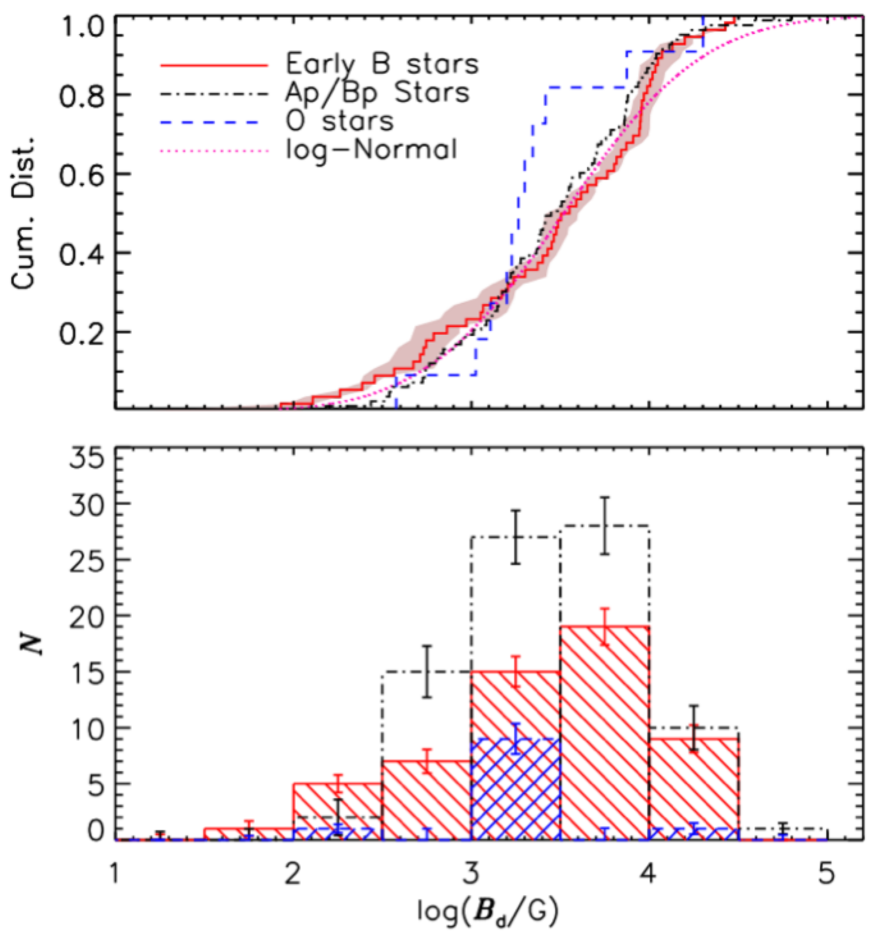

Shultz+2019a

How do we model these magnetic winds?

Wind confinement in magnetic B-stars

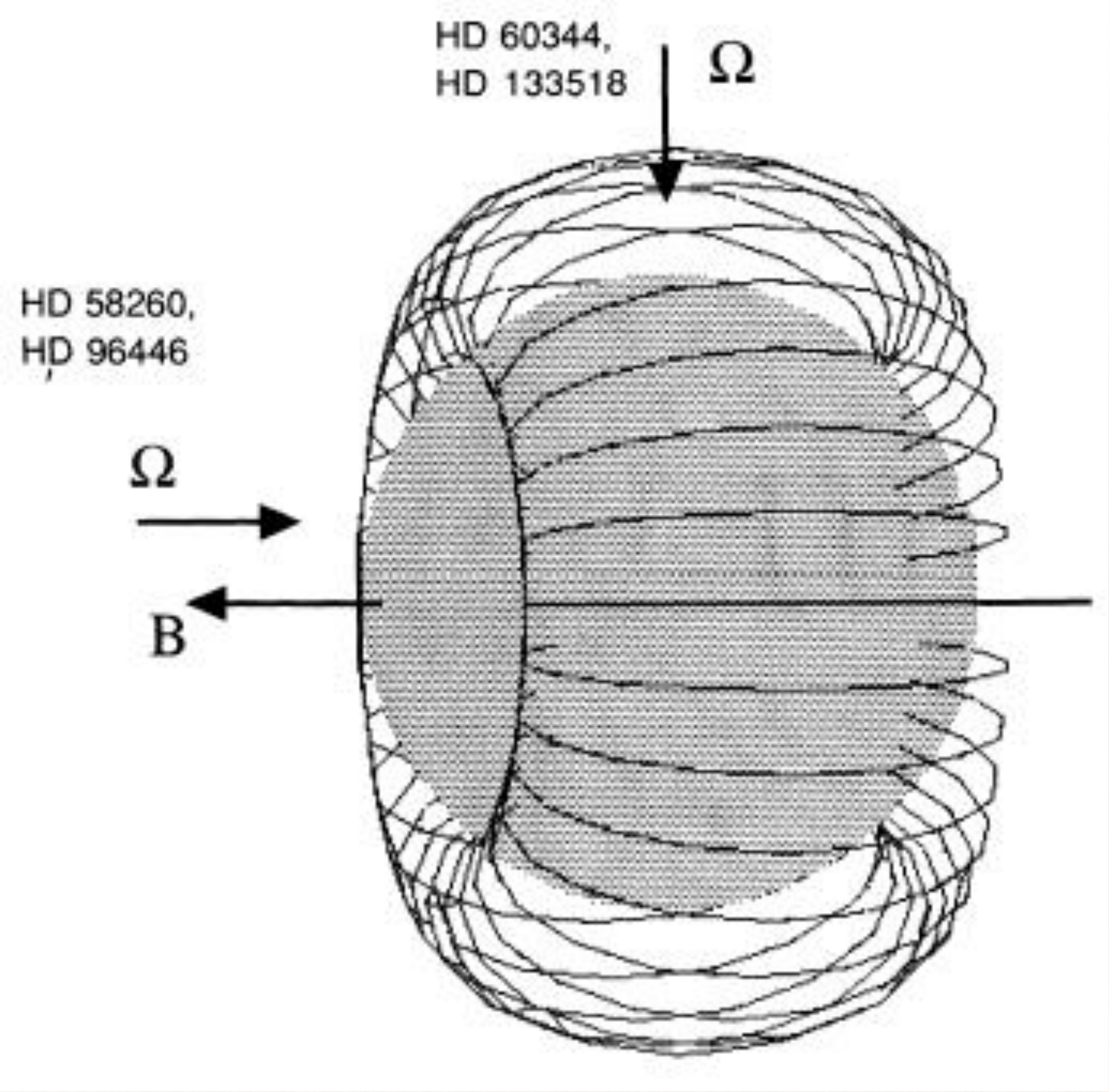

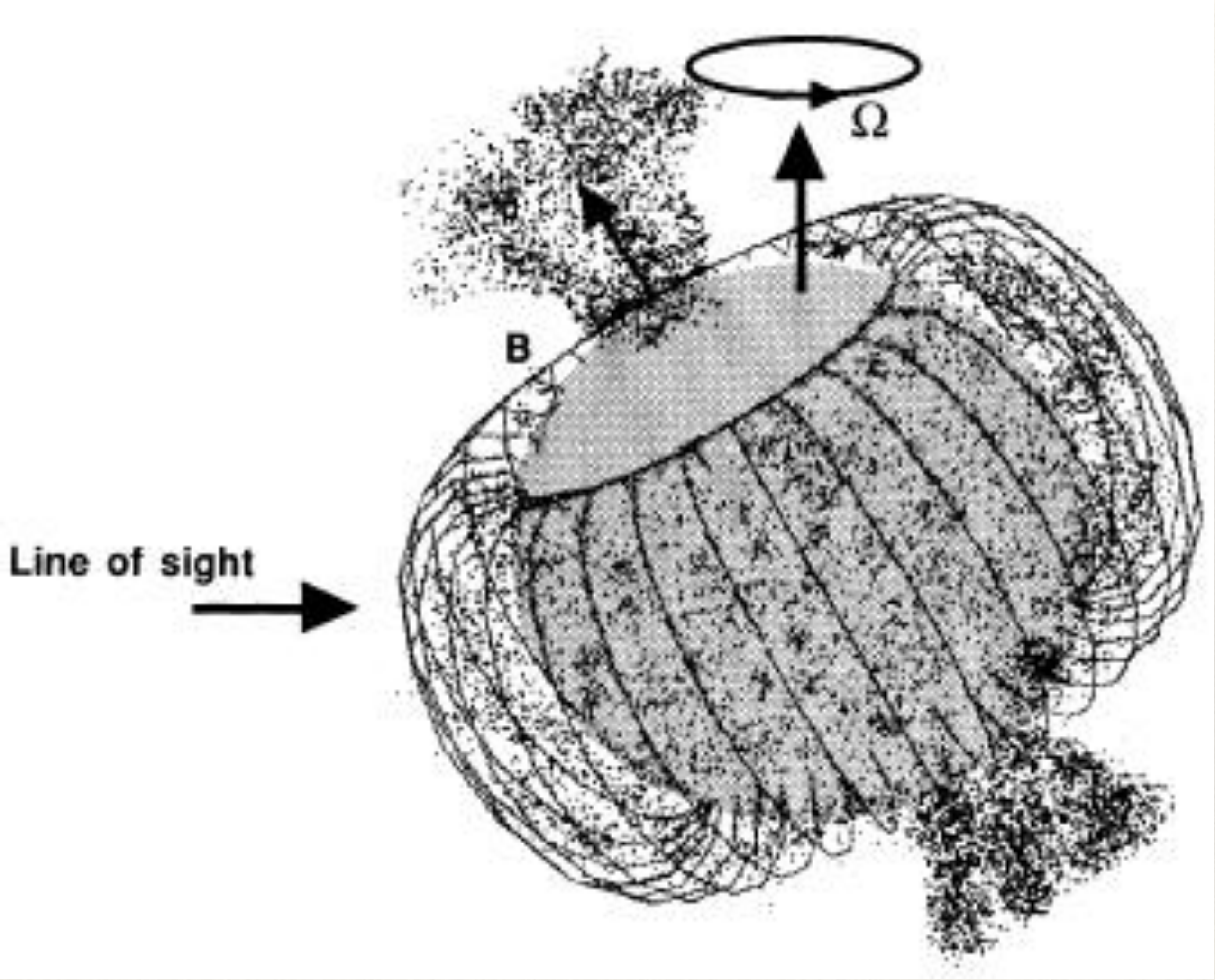

Shore & Brown 1990

Wind confinement in magnetic B-stars

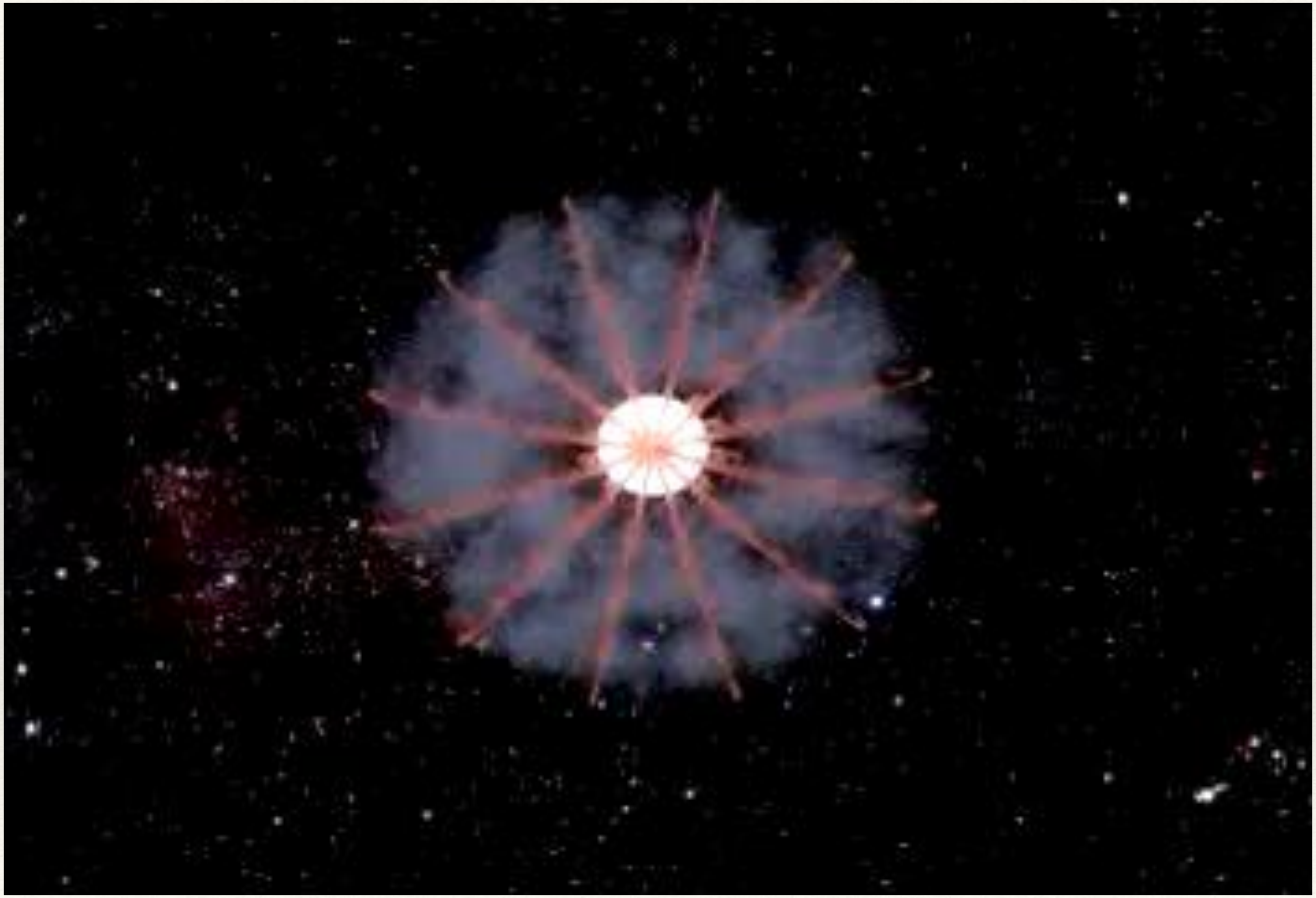

Magnetically Confined Wind-Shocks

Magnetic Ap-Bp stars

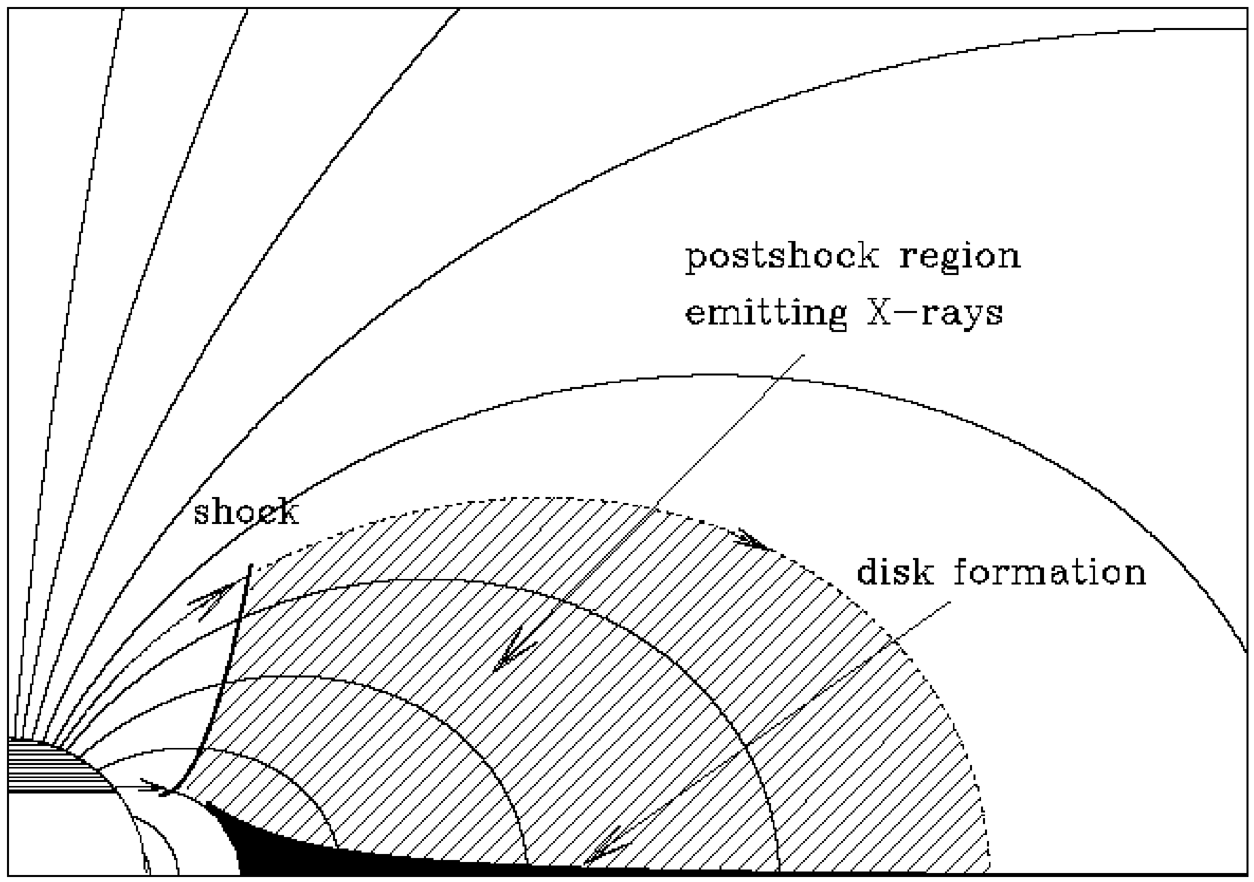

Fig. 7. Schematic view of the model proposed for the X-ray emission from IQ Aur (see text).

Babel & Montmerle 1997

Magnetic Confinement Parameter

$$\frac{\text{magnetic energy density}}{\text{kinetic energy density}} \quad \text{———} \quad \eta(r) \equiv \frac{B^2/8\pi}{\rho v^2/2}$$

$$\eta(r) = \frac{B^2 r^2}{\dot{M} v} = \left[\frac{B_*^2 R_*^2}{\dot{M} v_\infty}\right] \left[\frac{(r/R_*)^{-2n}}{(1-(R_*/r))^\beta}\right]$$

η*

$$\eta_* = \frac{B_0^2 R_*^2}{\dot{M} v_\infty} = 0.4 \times \frac{B_{100}^2 R_{12}^2}{\dot{M}_{-6} v_8}$$

for solar wind, η *~ 40

but for O-stars, to get η *~ 1, need: B* ~ 300 G for ζ Pup

Computing Alfven Radius

$$\eta(r) = \eta_* \left[\frac{(r/R_*)^{-2n}}{(1-(R_*/r))^{\beta}} \right]$$

For hot stars, $\beta \sim 1$

For a dipole n=2

$$\frac{R_A}{R_*} \approx \eta_*^{1/4}$$

For Moderate Confinement Cases: MHD

93 G ; $\eta^* = 0.1$

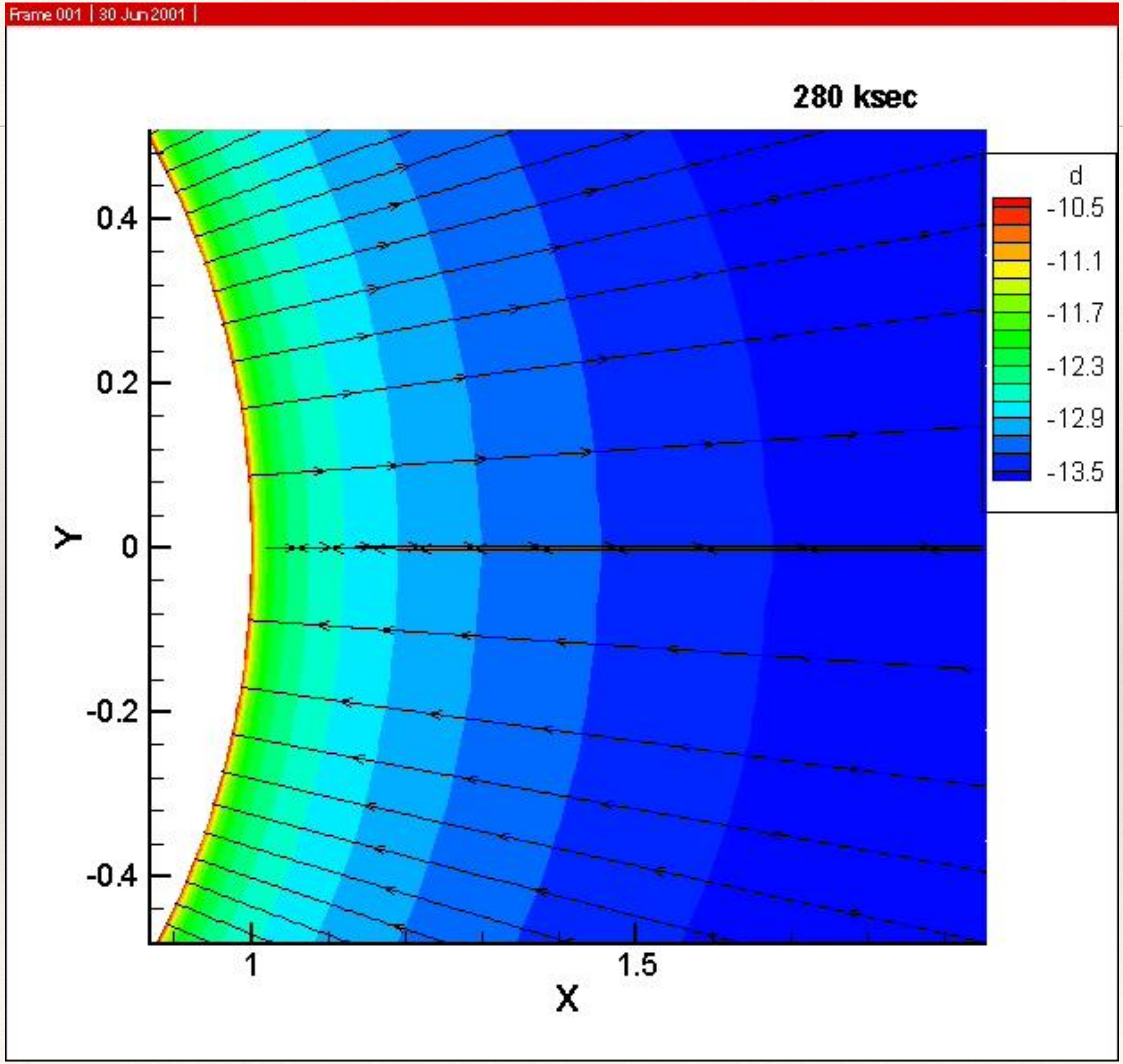

Zeus Code

520 G ; $\eta^* = 3.2$

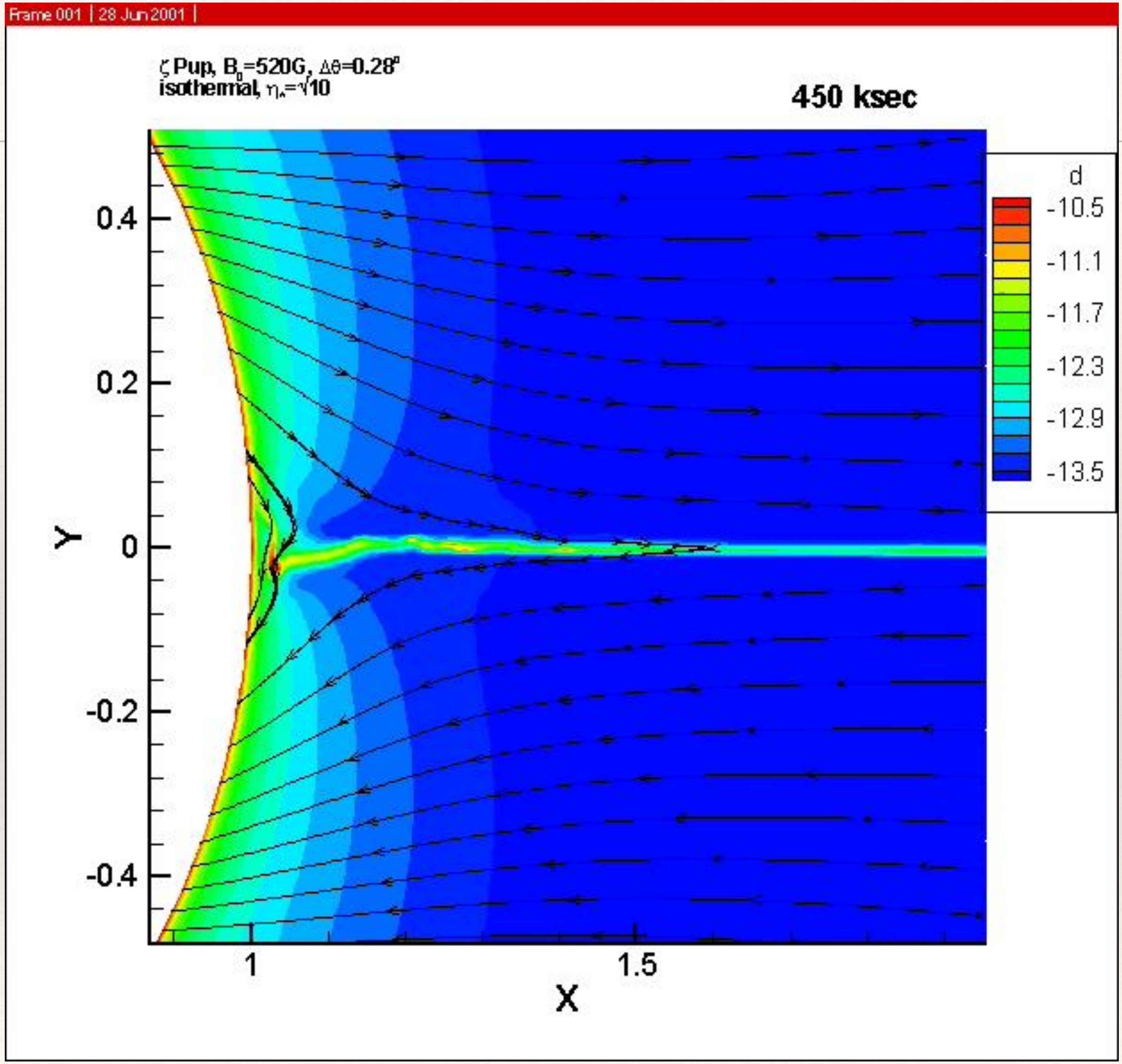

Frame 001 | 28 Jun 2001 |
ζ Pup, B0=520G, Δθ=0.28°
isothermal, η*=√10
450 ksec
d
-10.5
-11.1
-11.7
-12.3
-12.9
-13.5
0.4
0.2
0
-0.2
-0.4
Y
1
1.5
X

2950 G ; η* = 100

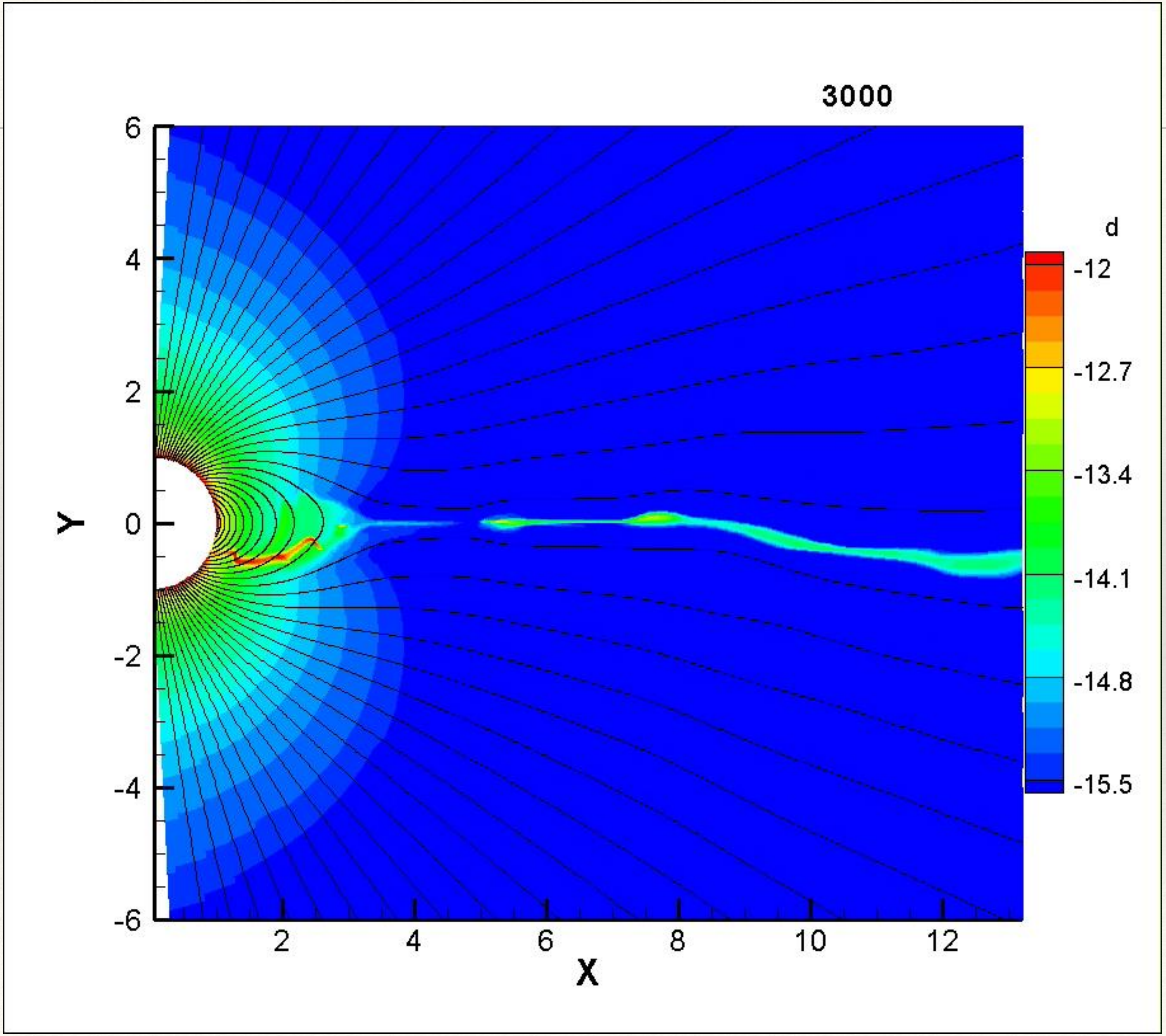

Magnetic confinement vs. Wind + Rotation

Wind mag. confinement

$$\eta_* = \frac{B_*^2 R_*^2}{\dot{M} v_\infty}$$

Rotation vs. critical

$$W = \frac{V_{rot}}{\sqrt{GM/R_*}}$$

Alfven radius

$$R_A = \eta_*^{1/4} R_*$$

Kepler radius

$$R_K = W^{-2/3} R_*$$

Centrifugal support

$$W = \frac{V_{rot}}{V_{crit}}$$

$$\frac{R_K}{R_*} \equiv W^{-2/3}$$

Kepler radius

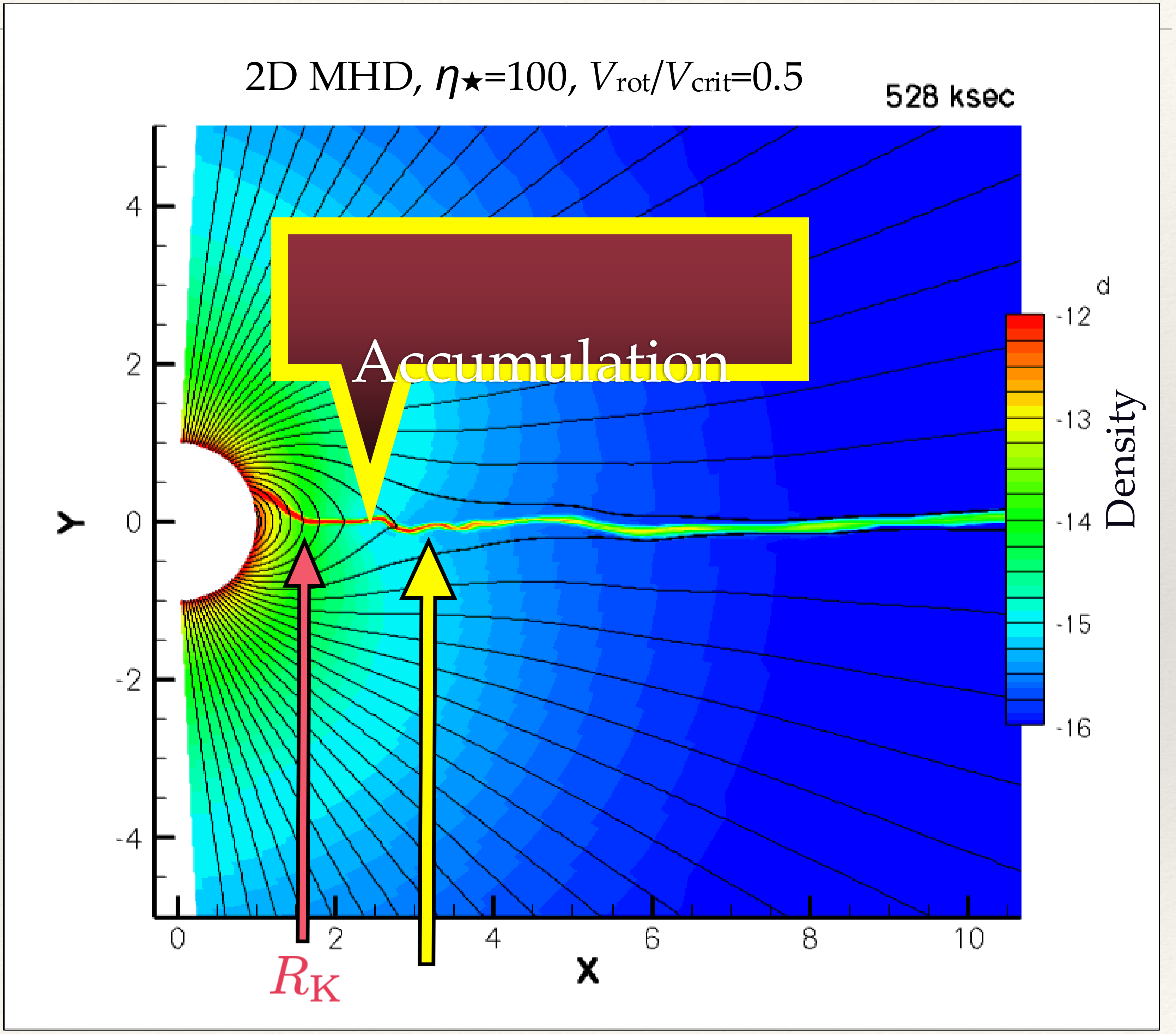

$$R_A \propto \eta_*^{1/4}$$

ud Doula+ 200

Radial Mass Distribution

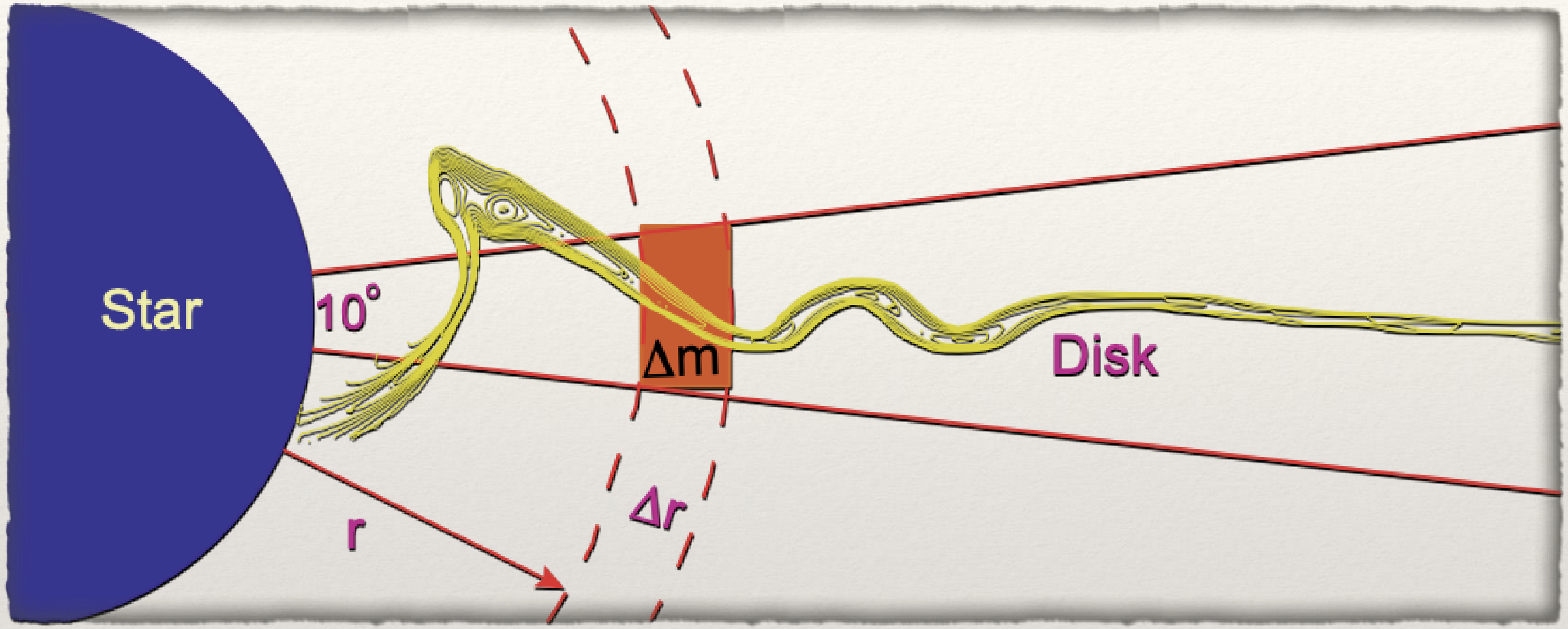

$$\frac{dm_{\mathrm{e}}(r,t)}{dr} \equiv 2\pi r^2 \int_{\pi/2-\Delta\theta/2}^{\pi/2+\Delta\theta/2} \rho(r,\theta,t)\,\sin\theta\,d\theta$$

Time evolution of Radial distribution of equatorial disk mass

$\eta^* = 100$ & Vrot/Vcrit =1/2

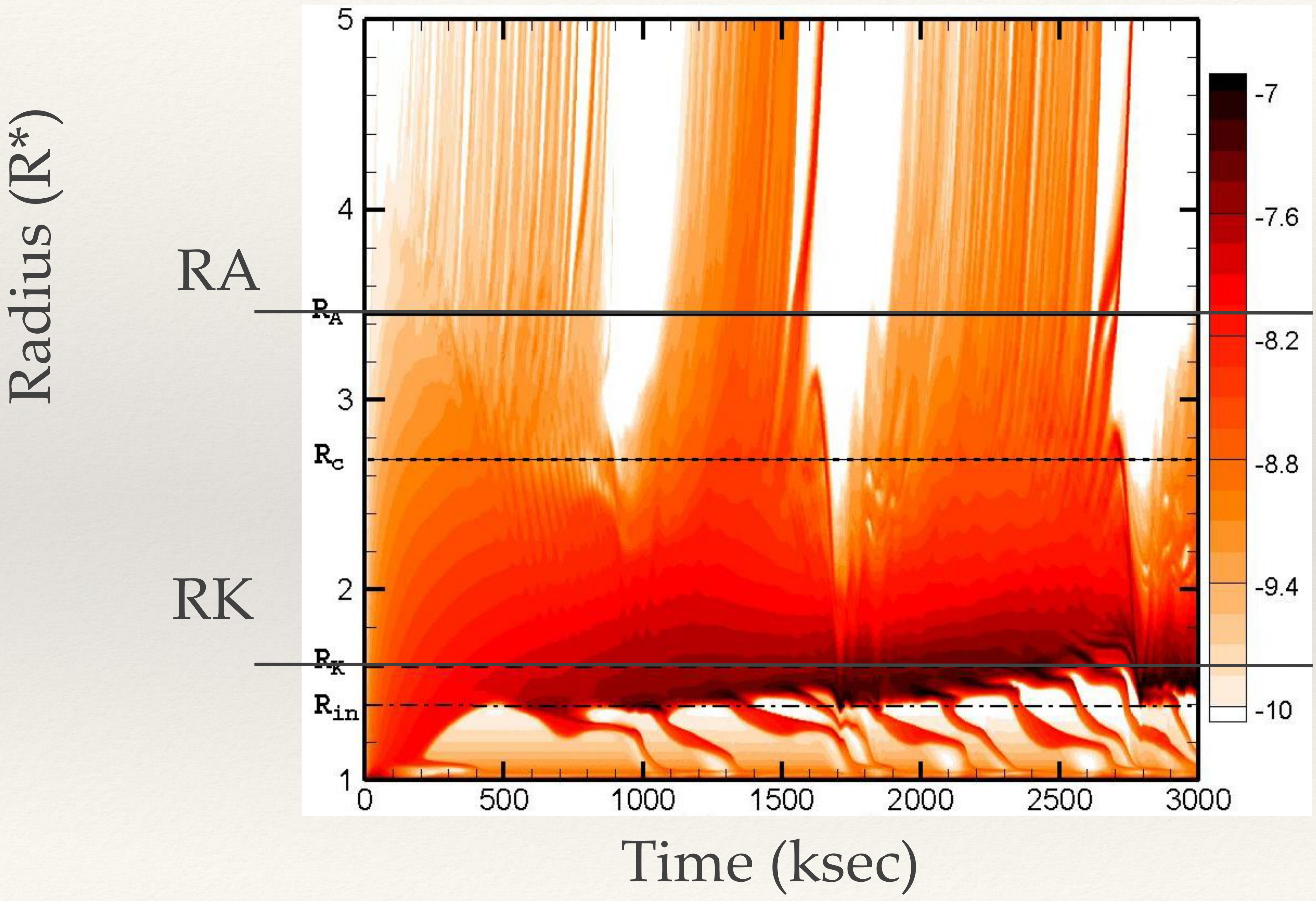

Two Parameter Study

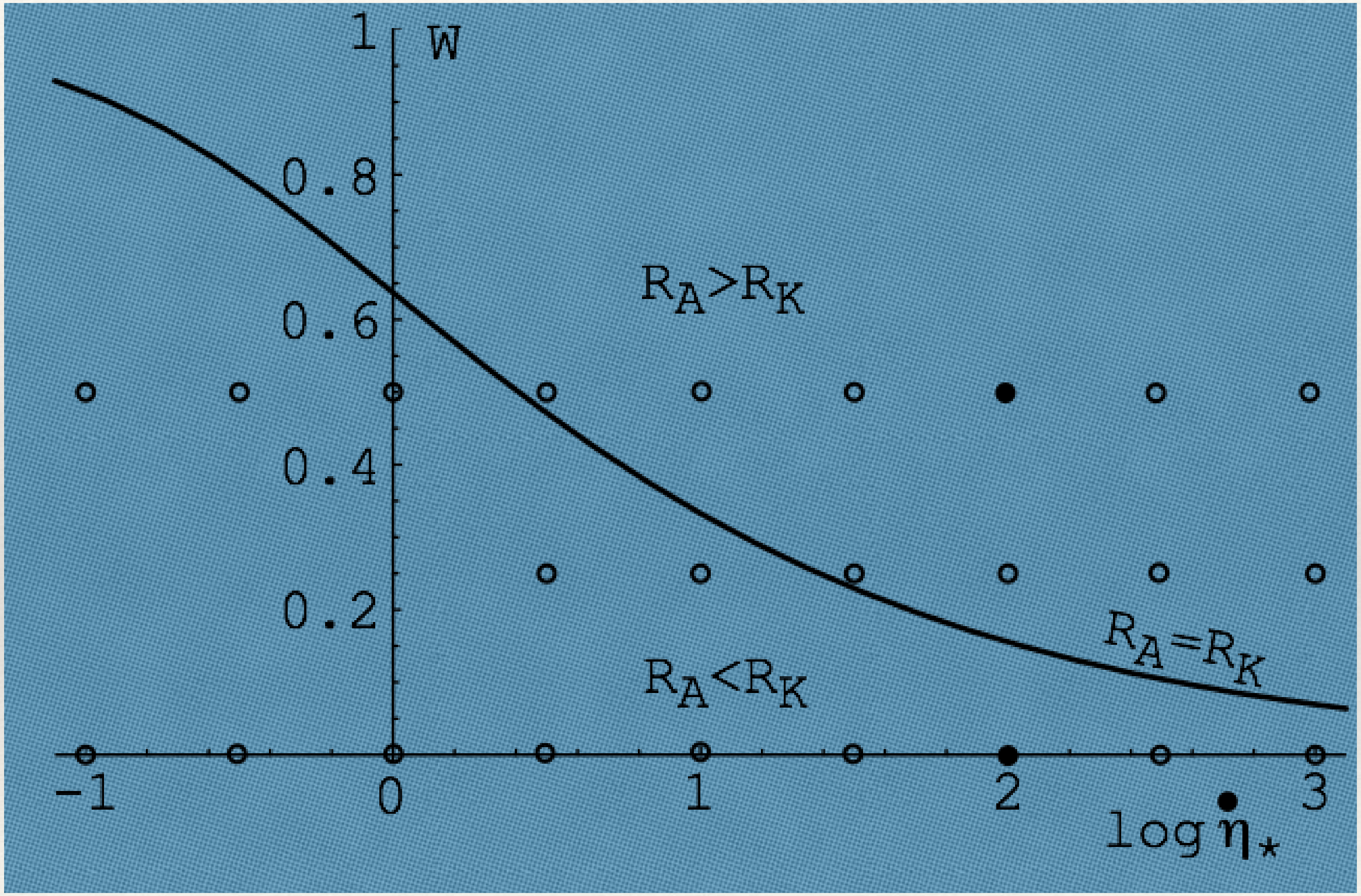

More Rapid Rotation --->

Stronger Magnetic Confinement --->

Radial Distribution of equatorial disk mass

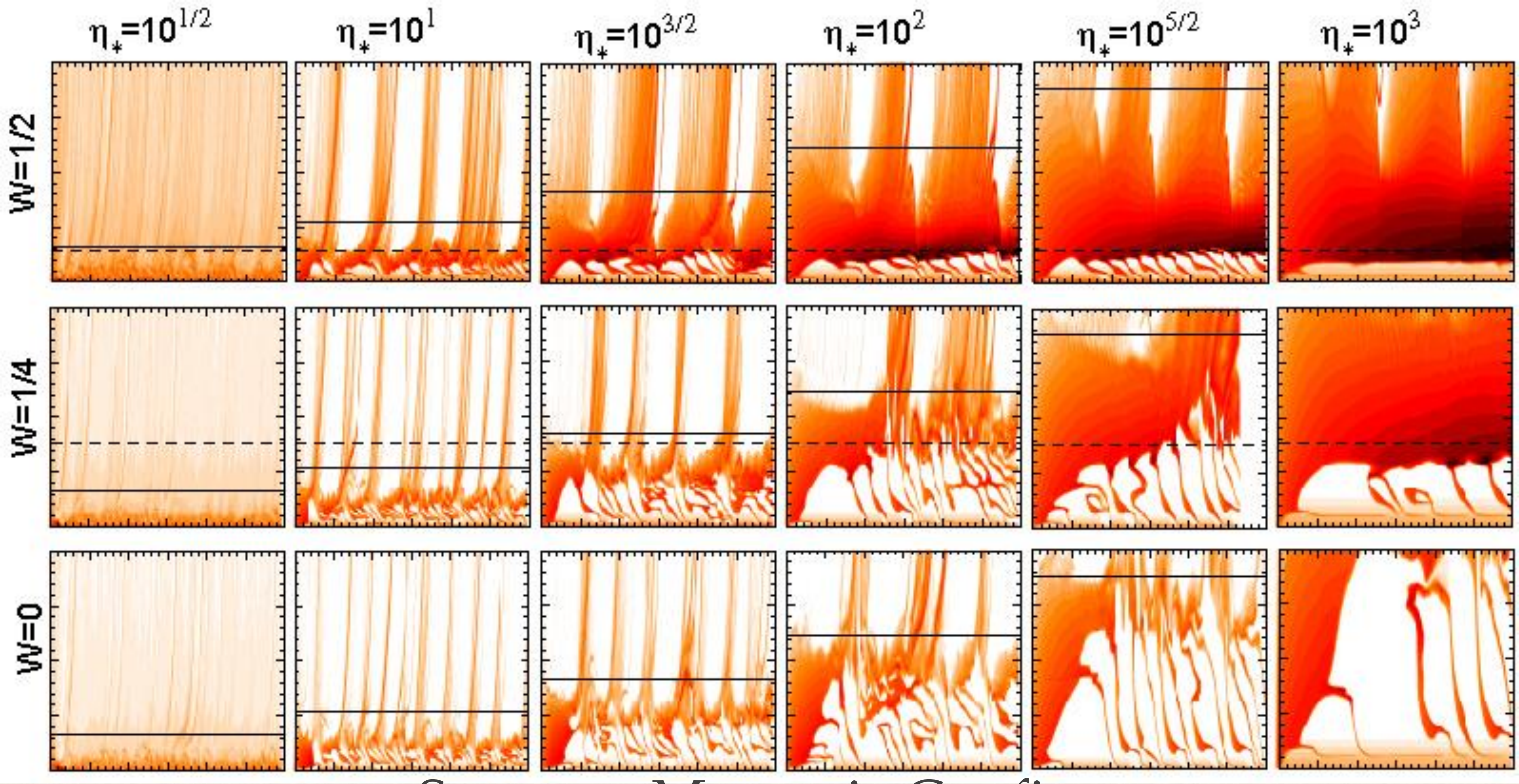

More Rapid Rotation --->

Stronger Magnetic Confinement --->

What are the implications?

Angular Momentum Loss

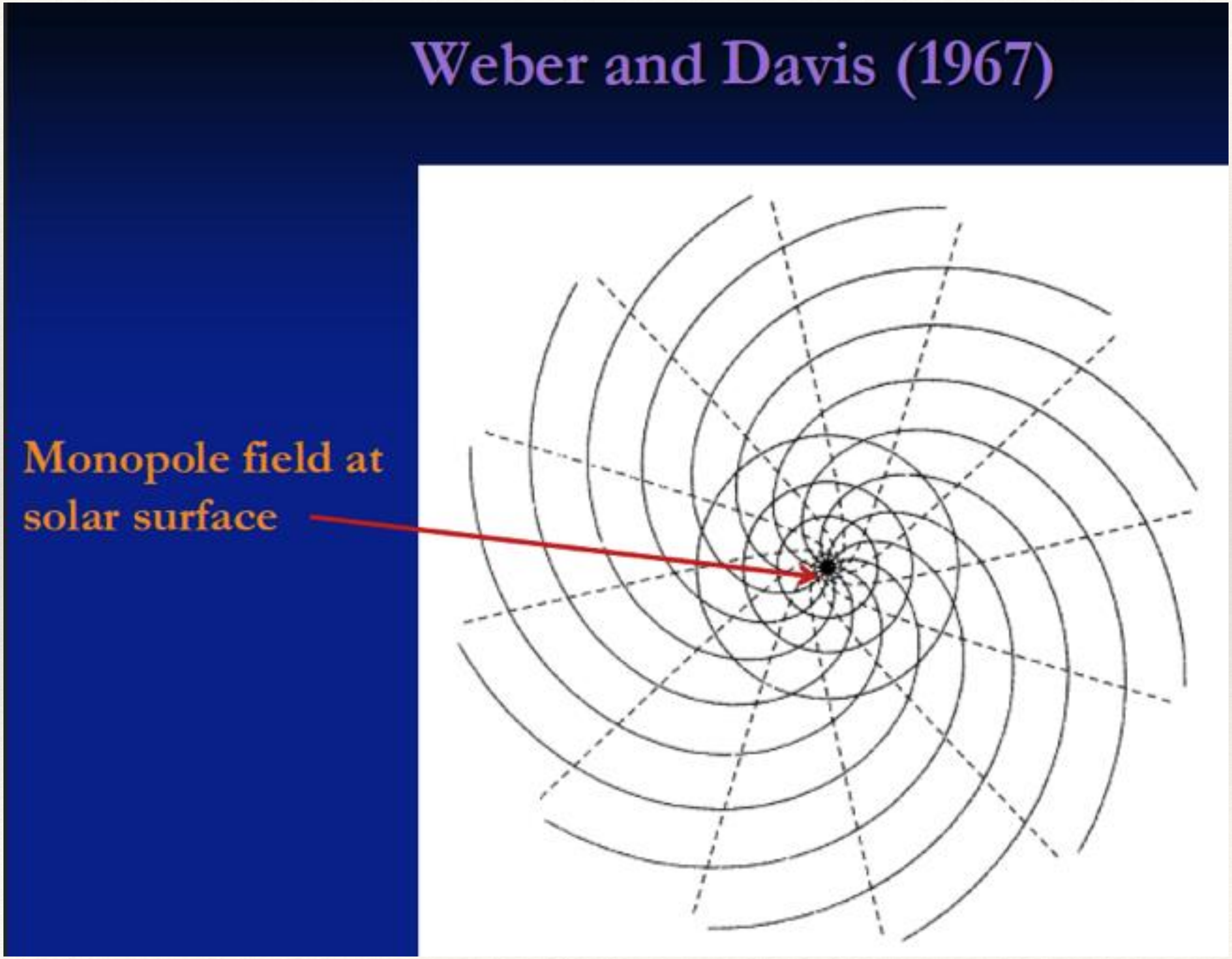

Spindown

contribution from both field and gas

$$\dot{J} = \frac{2}{3}\dot{M}\Omega R_A^2$$

For Dipole

$$\tau_{spin} \equiv \frac{J}{\dot{J}} \approx \frac{\frac{3}{2}I}{MR_*^2}\frac{M}{\dot{M}}\frac{1}{\sqrt{\eta_*}} = \tau_{mass}\frac{\frac{3}{2}k}{\sqrt{\eta_*}}$$

$$\frac{\tau_{spin}}{\tau_{mass}} = \frac{0.15}{\sqrt{\eta_*}}$$

Spindown Time

Table 1. Estimated spin-down time for selected known magnetic stars.

Star[a]	$M/\mathrm{M}_\odot$	$R_*/\mathrm{R}_\odot$	P (d)	k	$\dot{M}\,(10^{-9}\,\mathrm{M}_\odot\,\mathrm{yr}^{-1})$	$v_\infty\,(1000\,\mathrm{km\,s}^{-1})$	B_p (kG)	η_*	τ_spin (Myr)
θ^1 Ori C[1]	40	8	15.4	0.28	400	2.5	1.1	15.7	8
HD191612[2]	40	18	538	0.17	6100	2.5	1.6	7.6	0.4
ζ Cas[3]	8	5.9	5.37	0.1	0.3	0.8	0.34	3200	65.2
σ Ori E[4]	8.9	5.3	1.2	0.1	2.4	1.46	9.6	1.4×10^5	1.4
ρ Leo[5]	22	35	7-47	0.12	630	1.1	0.24	20	1.1

[a]References: [1]Donati et al. (2002); [2]Donati et al. (2006); [3]Neiner et al. (2003) and Smith & Bohlender (2007); [4]Krtička, Kubát & Groote (2006) and [5]Kholtygin et al. (2007).

ud-Doula et al. 2009

Rotational Braking of σ Ori E

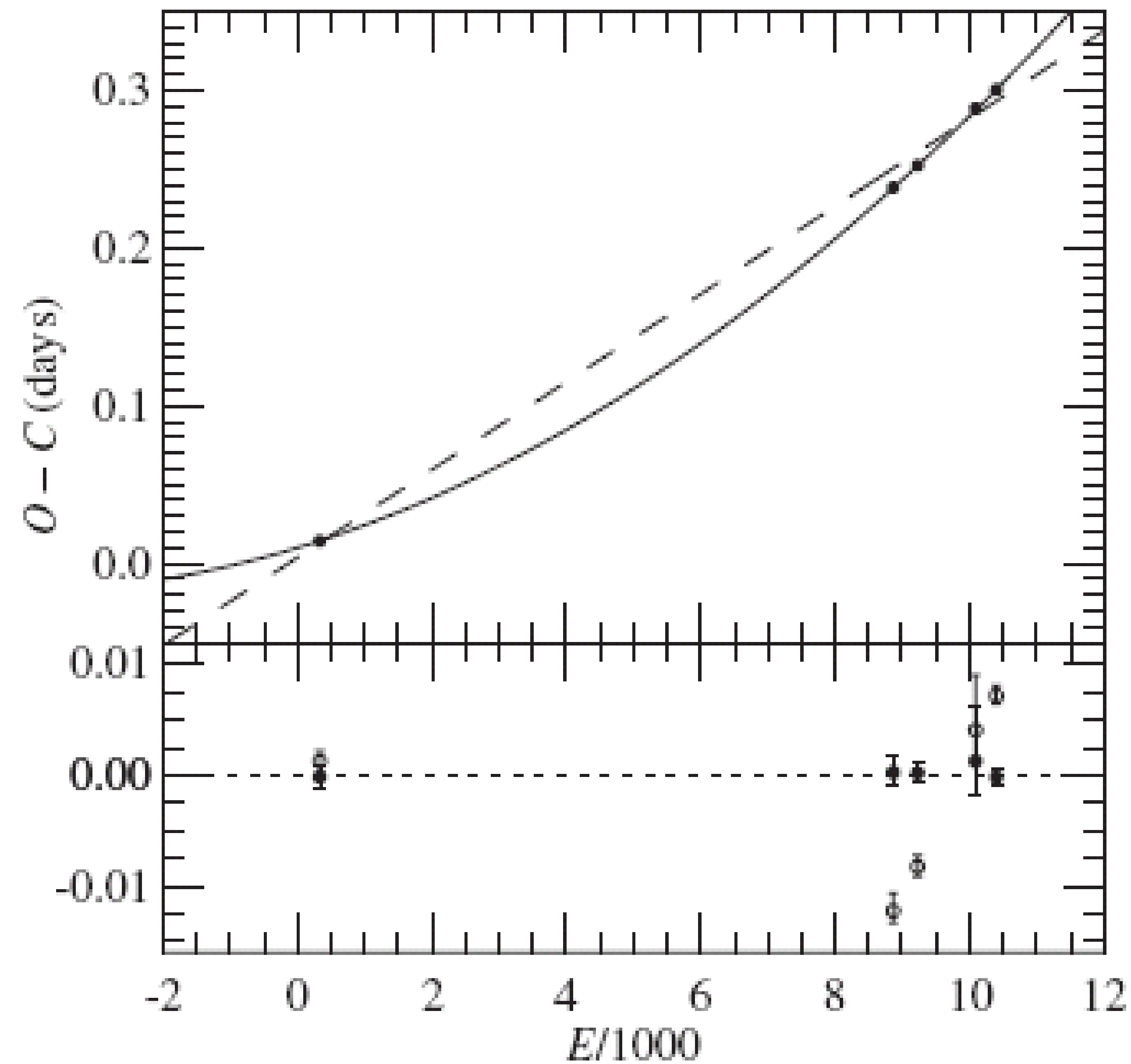

Figure 3. Observed-minus-corrected diagram for the primary minimum measurements. The solid (dashed) lines indicate the best-fit quadratic (linear) models; the residuals relative to these models are shown below the $O - C$ diagram as filled (open) symbols.

Predicted

τspin=1.40 Myr

Measured

τspin=1.34 Myr

Townsend et al. 2010

Non-isothermal 2D models: X-ray

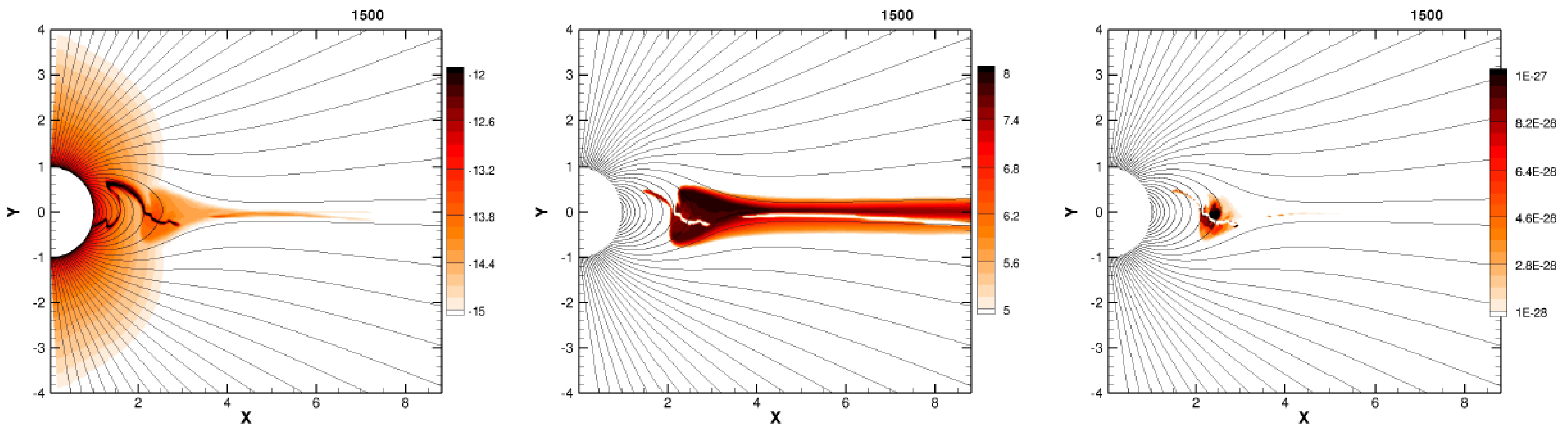

Figure 4. Color plots of log density (left) and log temperature (middle) for arbitrary snapshot of structure in the standard model with $\eta_* = 100$ and no IC cooling. The right panel plots the proxy X-ray emission XEM_{T_x} (weighted by the radius r) from (26), on a *linear* scale for a threshold X-ray temperature $T_x = 1.5\,\mathrm{MK}$.

ud-Doula et al. 2014

X-ray Emission Measure

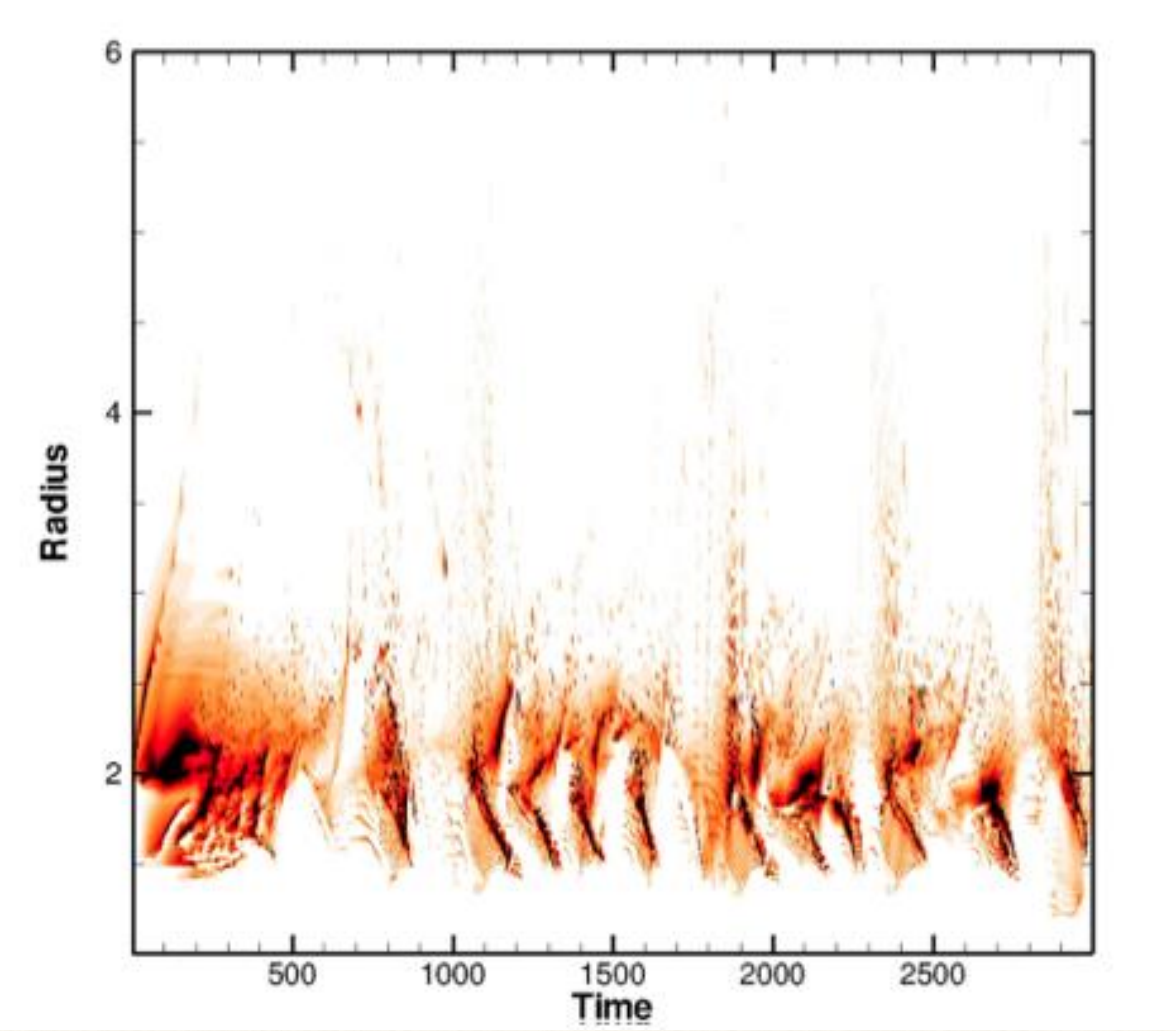

ud-Doula et al. 2014

X-ray from magnetic stars

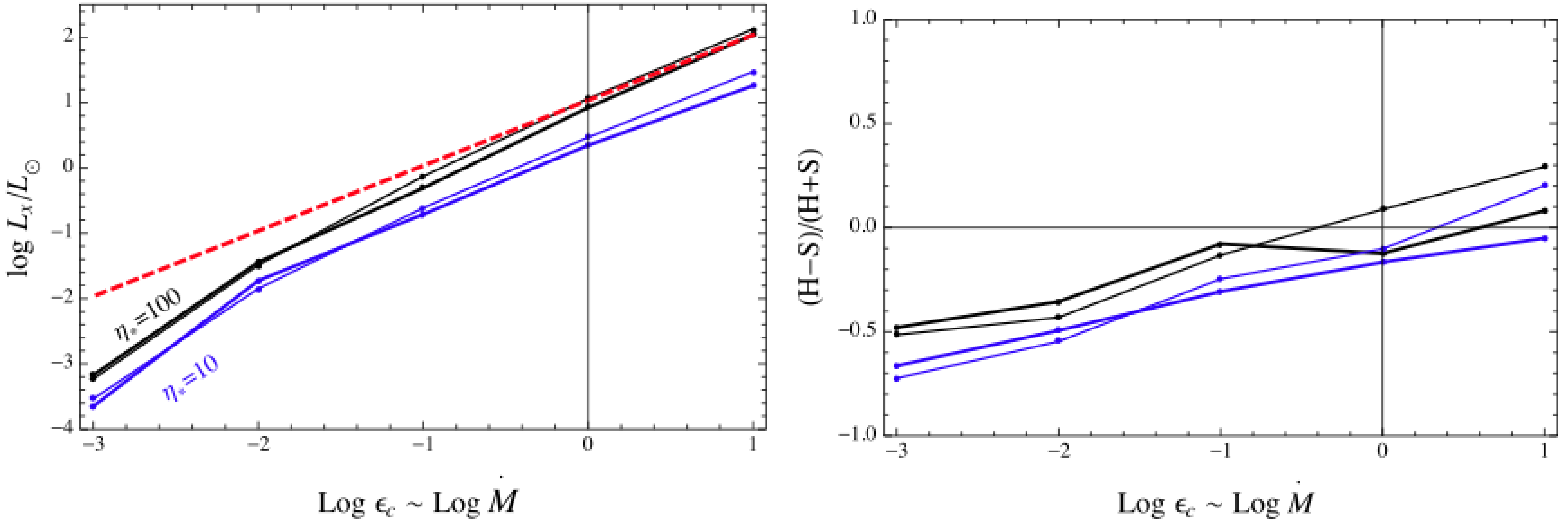

Figure 9. Left: log of time-averaged X-ray luminosity, log $L_{\rm x}$, for X-rays above $E_{\rm x} = 0.3$ keV, plotted versus log of cooling efficiency log $\epsilon_{\rm c}$, which acts as a proxy for mass-loss rate $\dot{M}$. The upper (black) and lower (blue) curves are, respectively, for $\eta_* = 100$ and $\eta_* = 10$, and the thick and normal thickness lines represent models with and without IC cooling. The dashed red line shows a linear relation normalized to values for the $\eta_* = 100$ model with the strongest cooling $\epsilon_{\rm c} = 10$. Right: analogous plots of hardness ratio (H−S)/(H+S) versus log $\epsilon_{\rm c}$, where H represents emission from 1 to 10 keV, and S represents emission from 0.3 to 1 keV.

ud-Doula et al. 2014

Observed X-ray

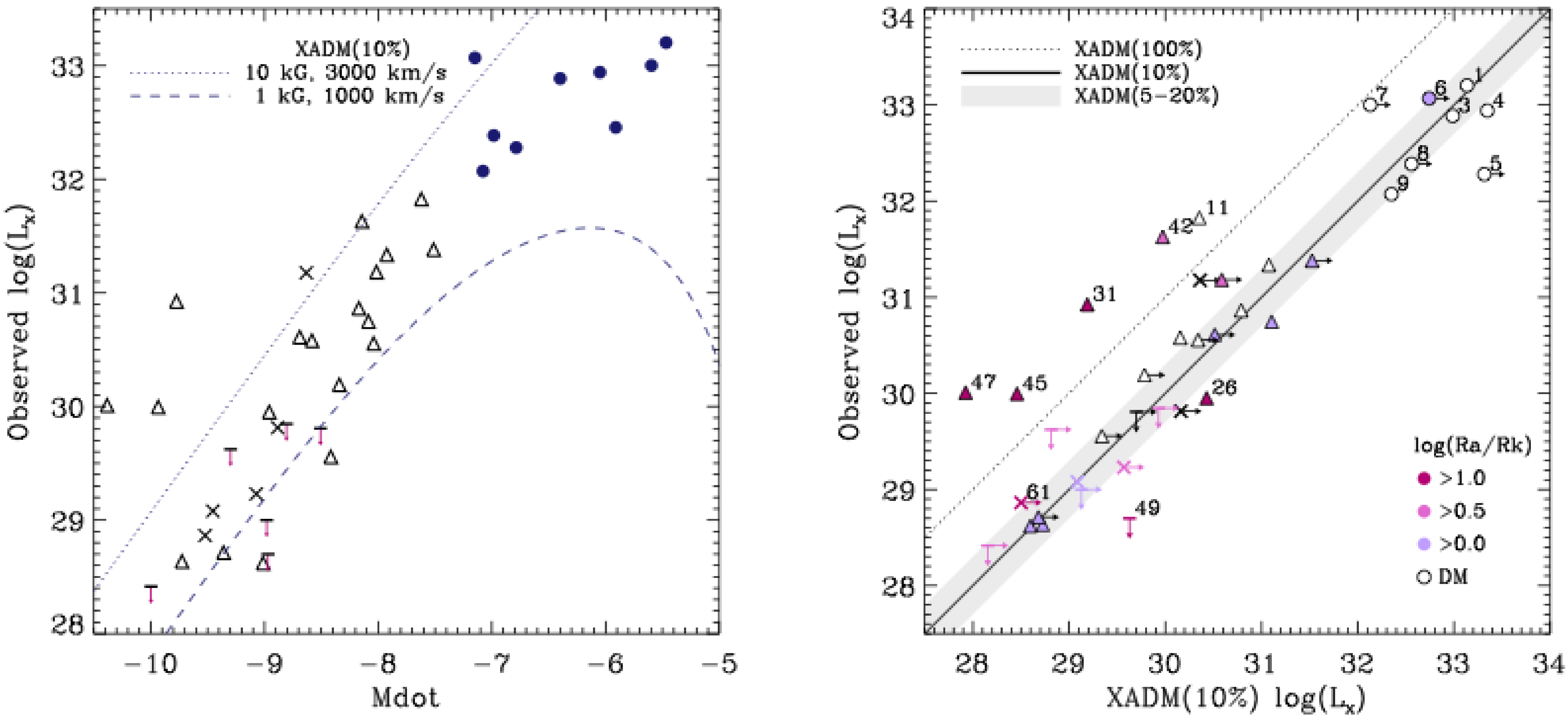

Nazé et al. 2014

For Strong Confinement Cases

($\eta_* >> 1 \rightarrow \infty$) : RRM, RFHD, ARFHD

Effective Gravitational+Centrifugal Potential

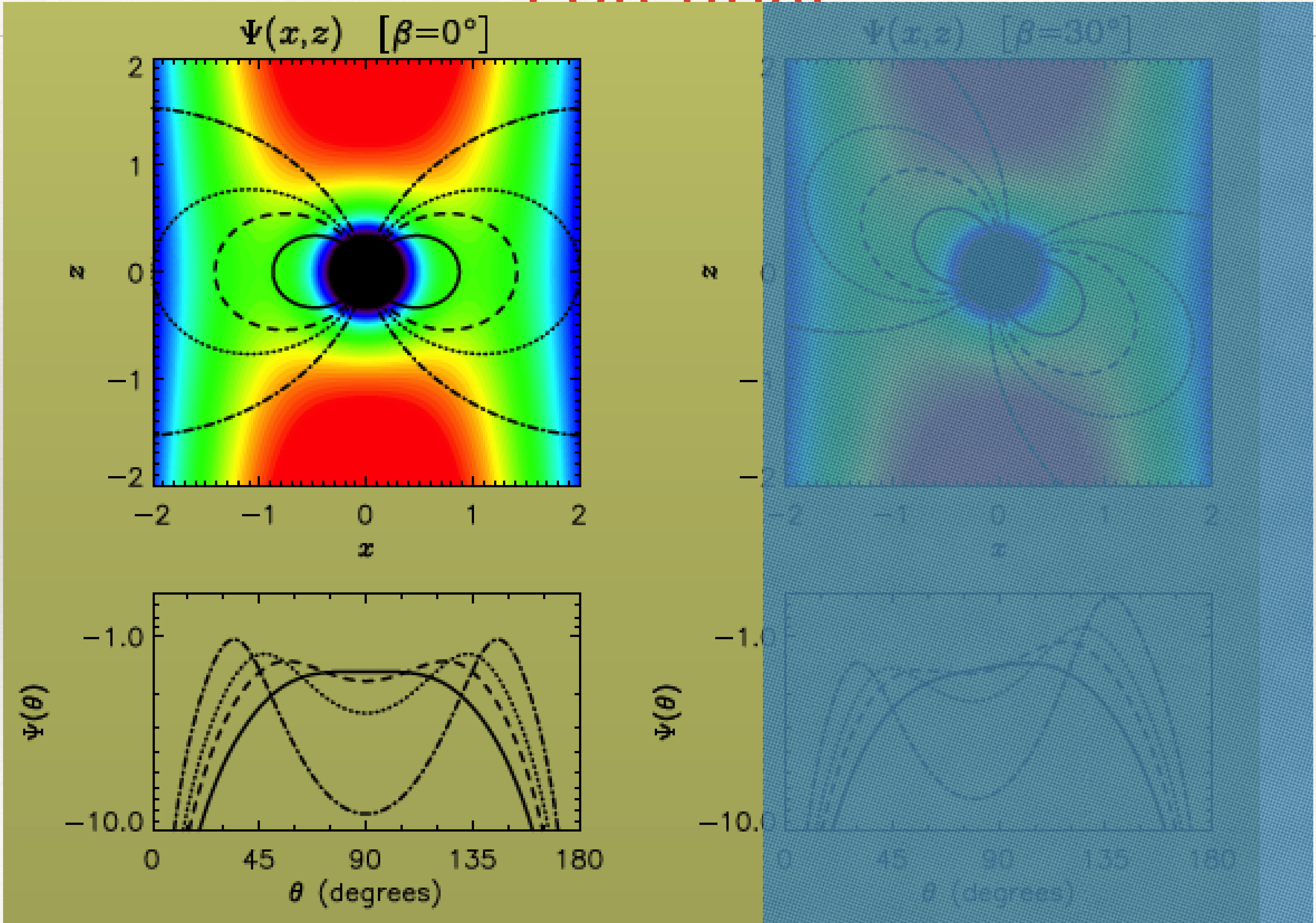

Rigidly Rotating Magnetosphere

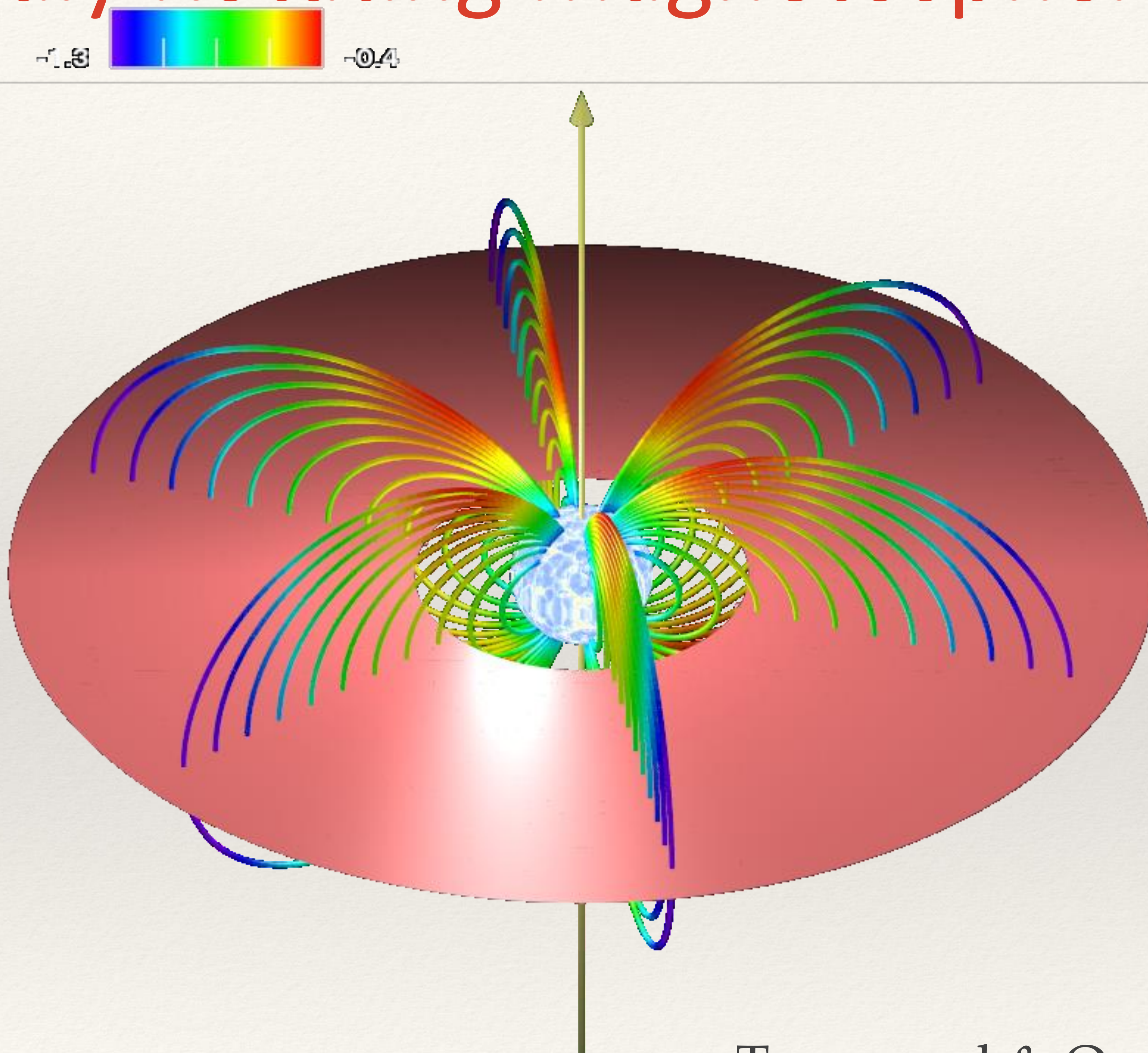

Townsend & Owocki (2005)

β=30o β=60o β=90o

Rotational phase ---->

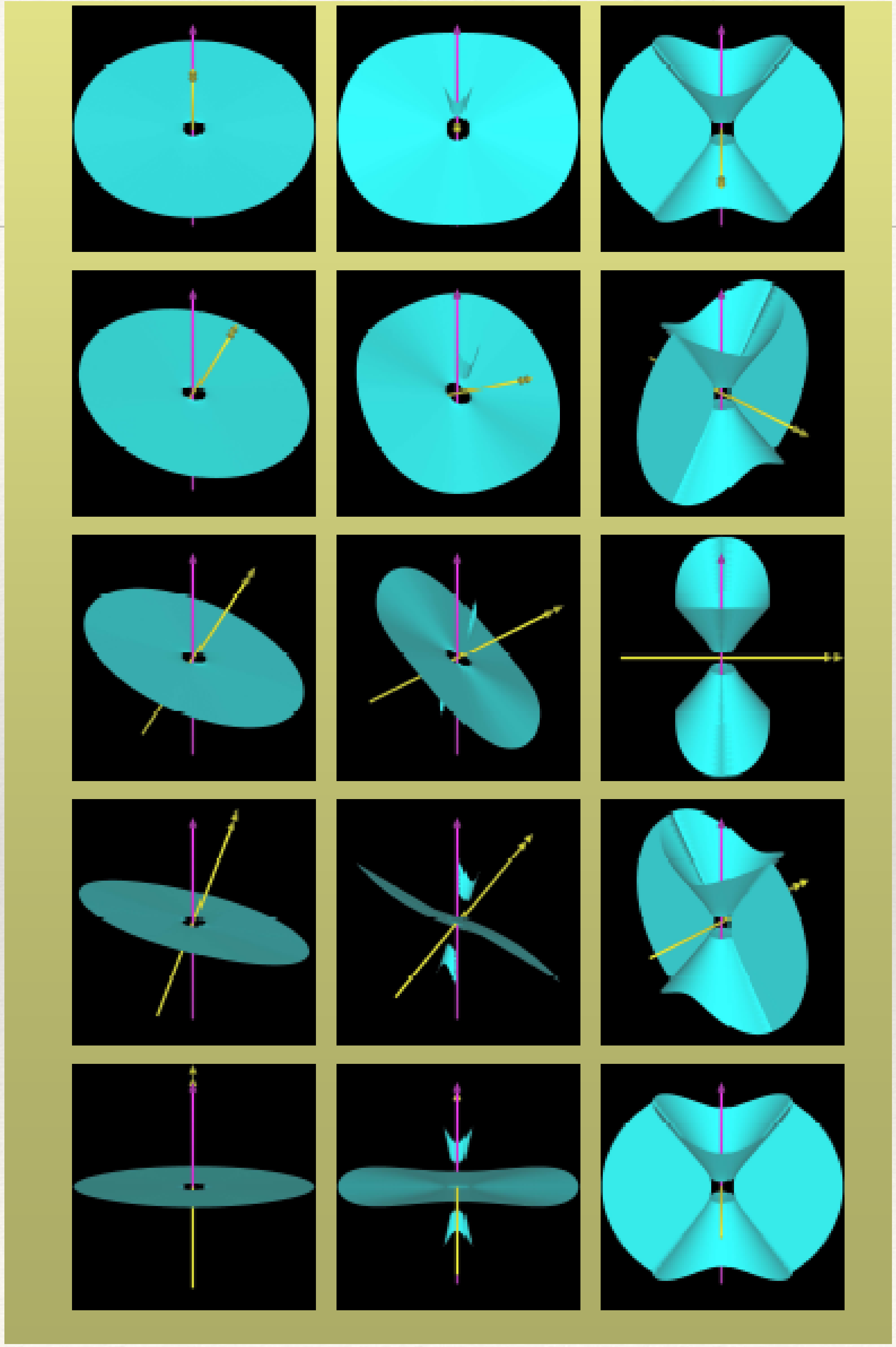

photometry

RRM model for σ Ori E

$B^* \sim 10^4$ G

$\eta^* \sim 10^6$!

tilt ~ 55 $^{\text{deg}}$

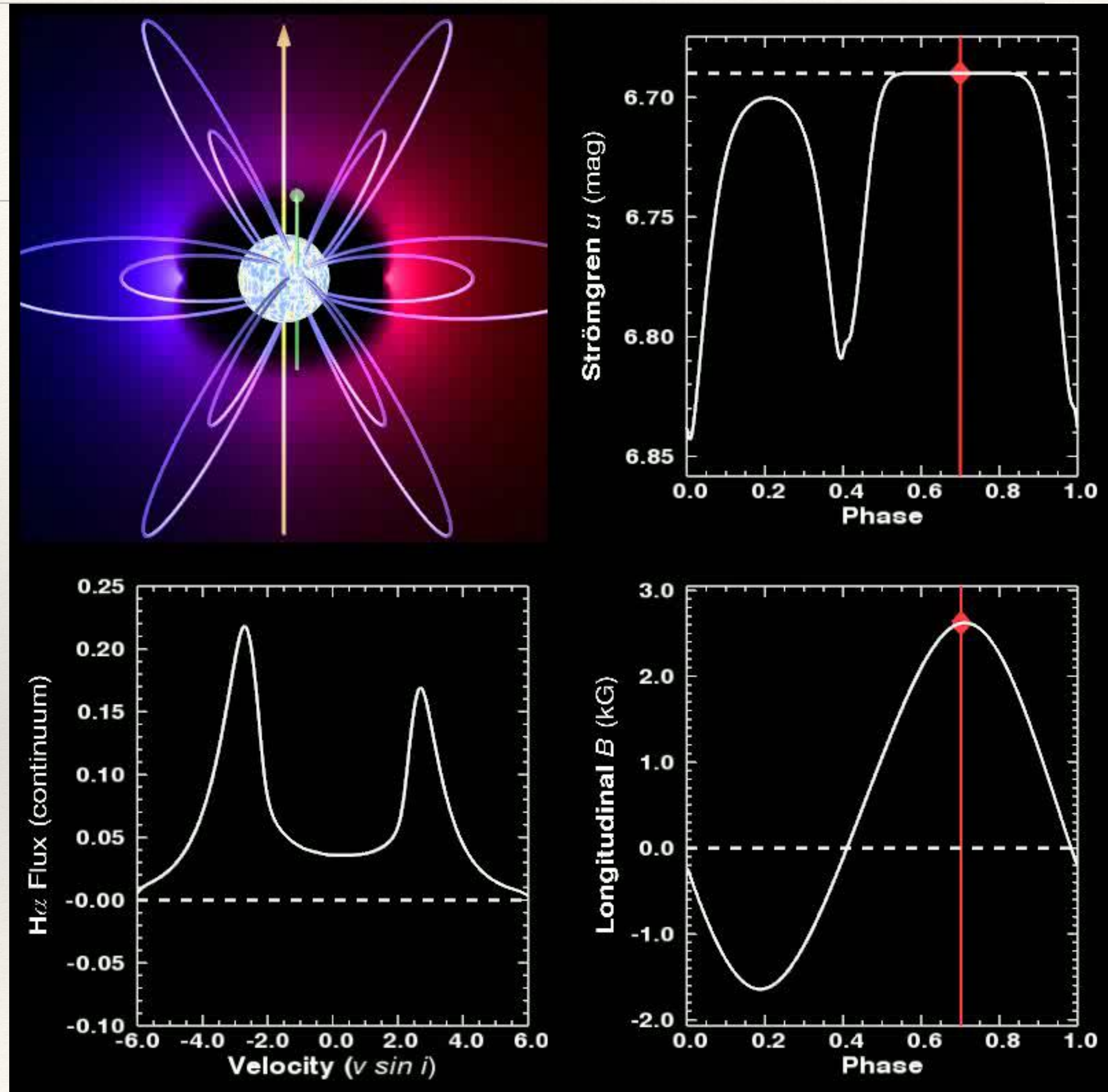

Hα

polarimetry

σ Ori E

RRM Model

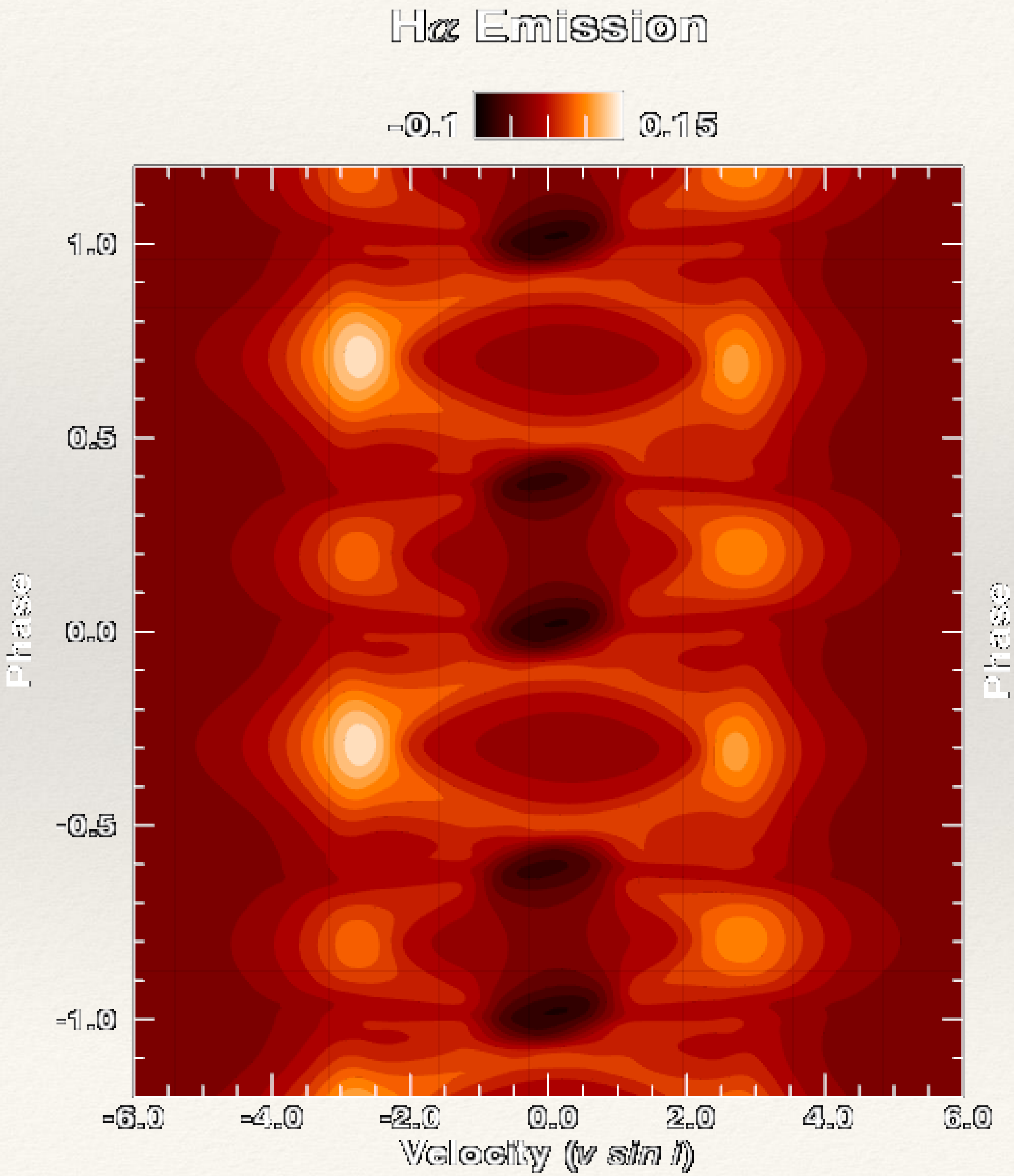

Hα Observations

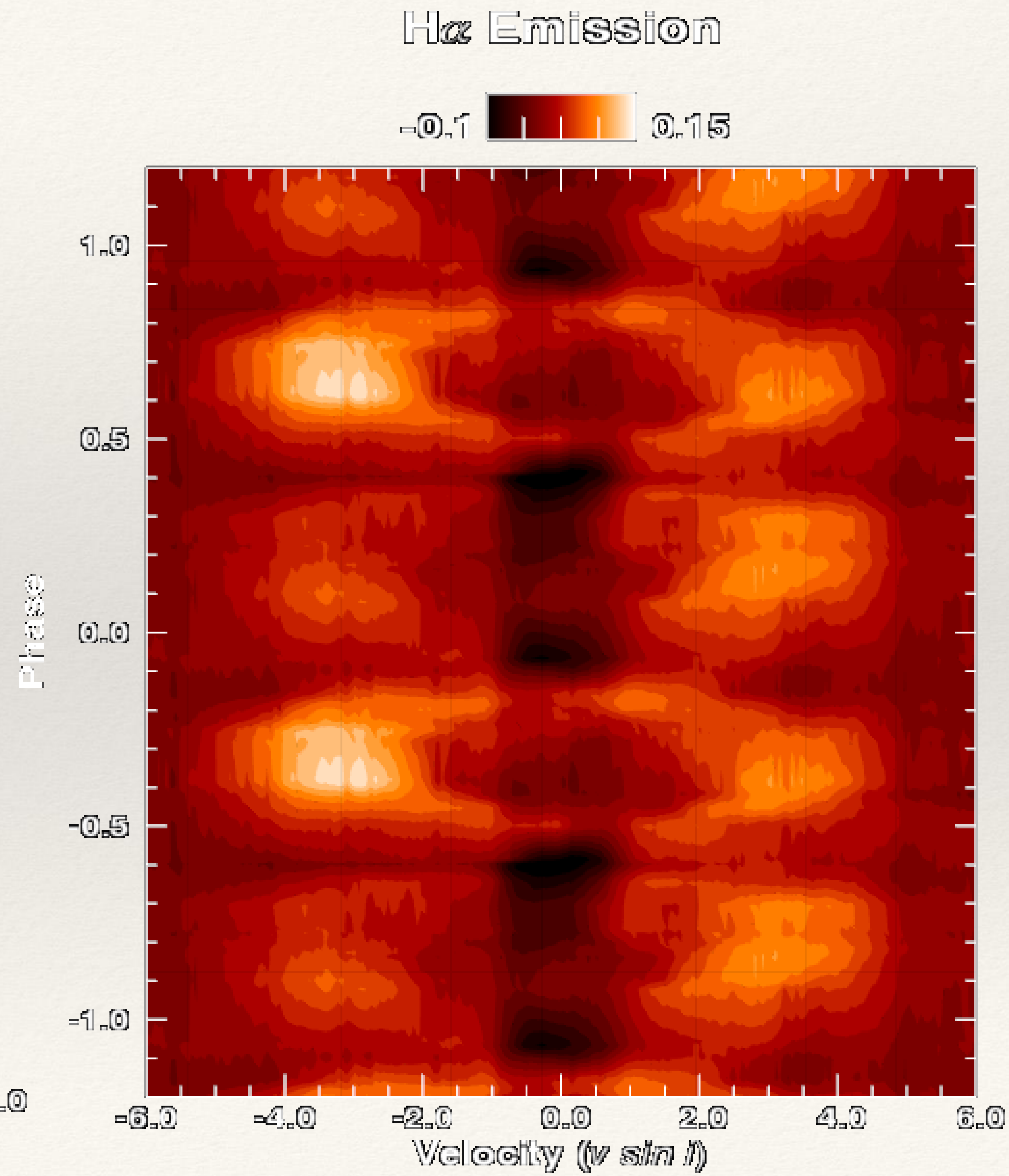

ARBITRARY-FIELD RRM (ARRM)

Oksala et al. 2016

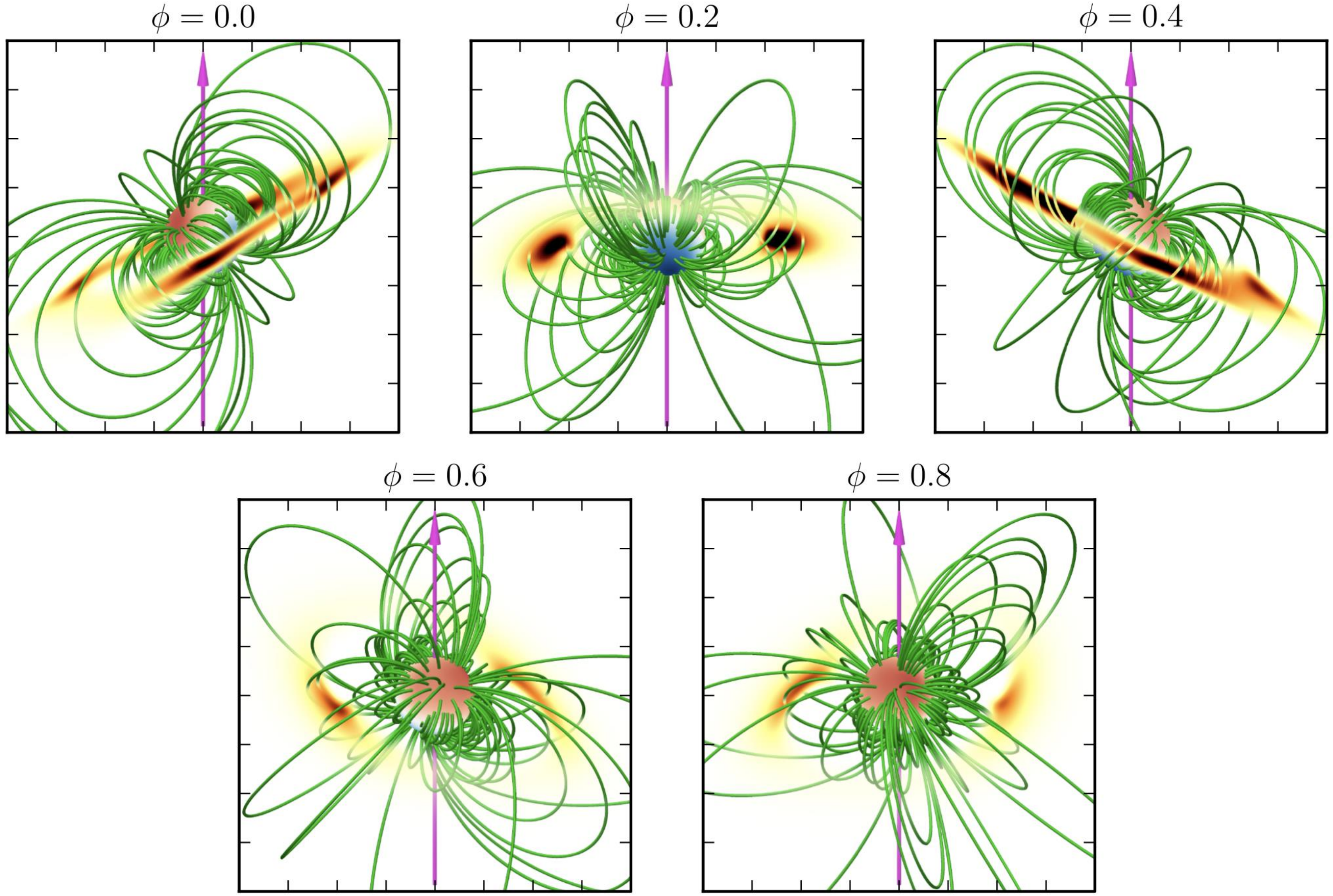

Figure 7. Visualizations of the plasma distribution predicted by the ARRM model, at the same five rotational phases adopted in previous figures. The star is coloured according to the radial magnetic field strength, as in the middle panels of Fig. 2; selected field lines are plotted in green, and the magenta arrow shows the star's rotation axis. The surrounding distribution of magnetospheric material is shown via an orange-coloured volume rendering, with the more opaque parts corresponding to higher column densities and vice versa. The tick marks on the surrounding boxes are spaced by $1R_*$.

IMPROVED RRM (ARRM)

Oksala et al. 2016

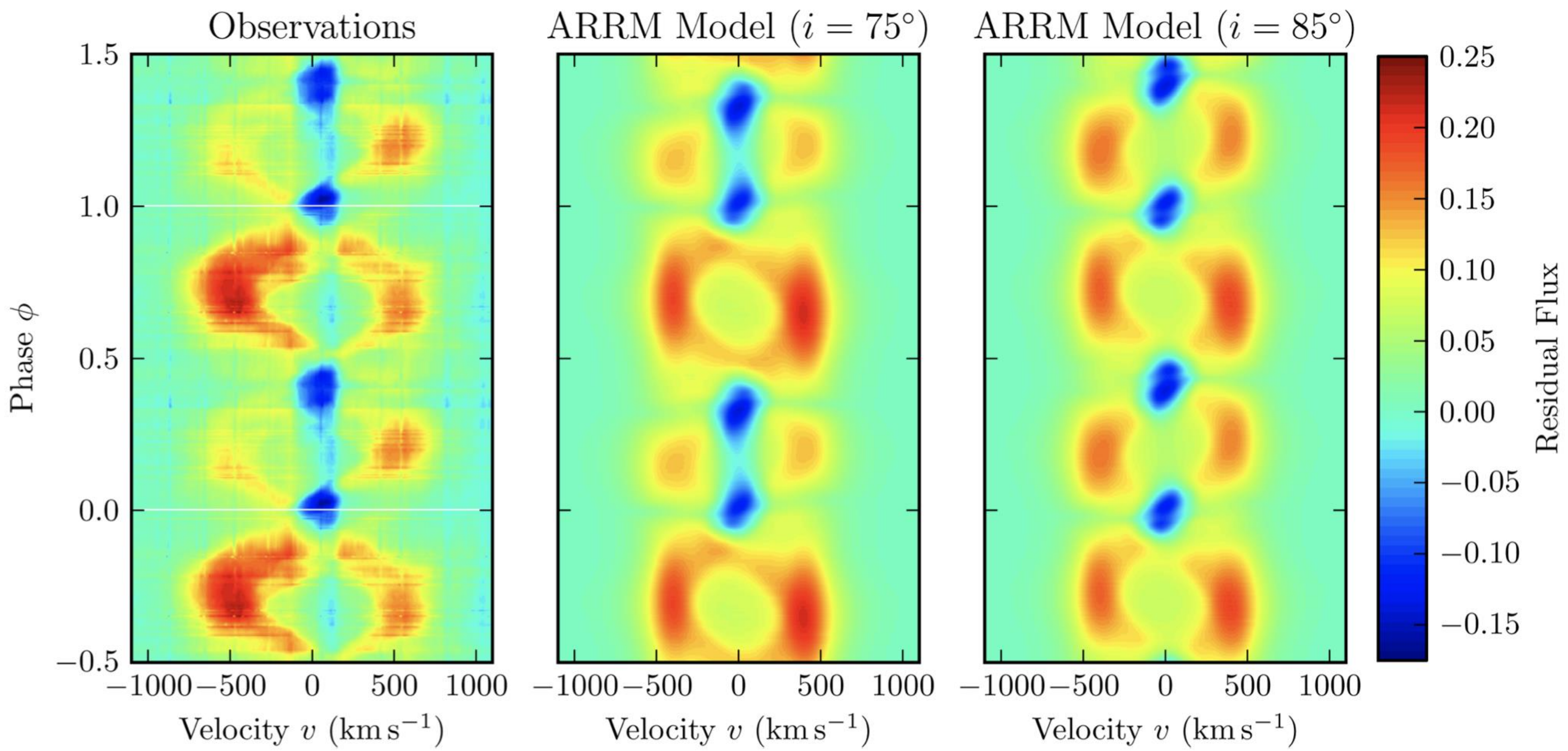

Figure 9. Comparison between observed (left) and modelled (middle and right) H α dynamic spectra of σ Ori E, in each case plotting the residual flux as a function of velocity and rotation phase. The middle plot is determined for an inclination angle, $i = 75°$, while the right-hand plot is the same, but for $i = 85°$. The observational data and the synthetic reference spectrum used to calculate the residuals are described in section 4 of Paper I.

Rigid Field - Hydro Model

Townsend, Owocki and ud-Doula (2007)

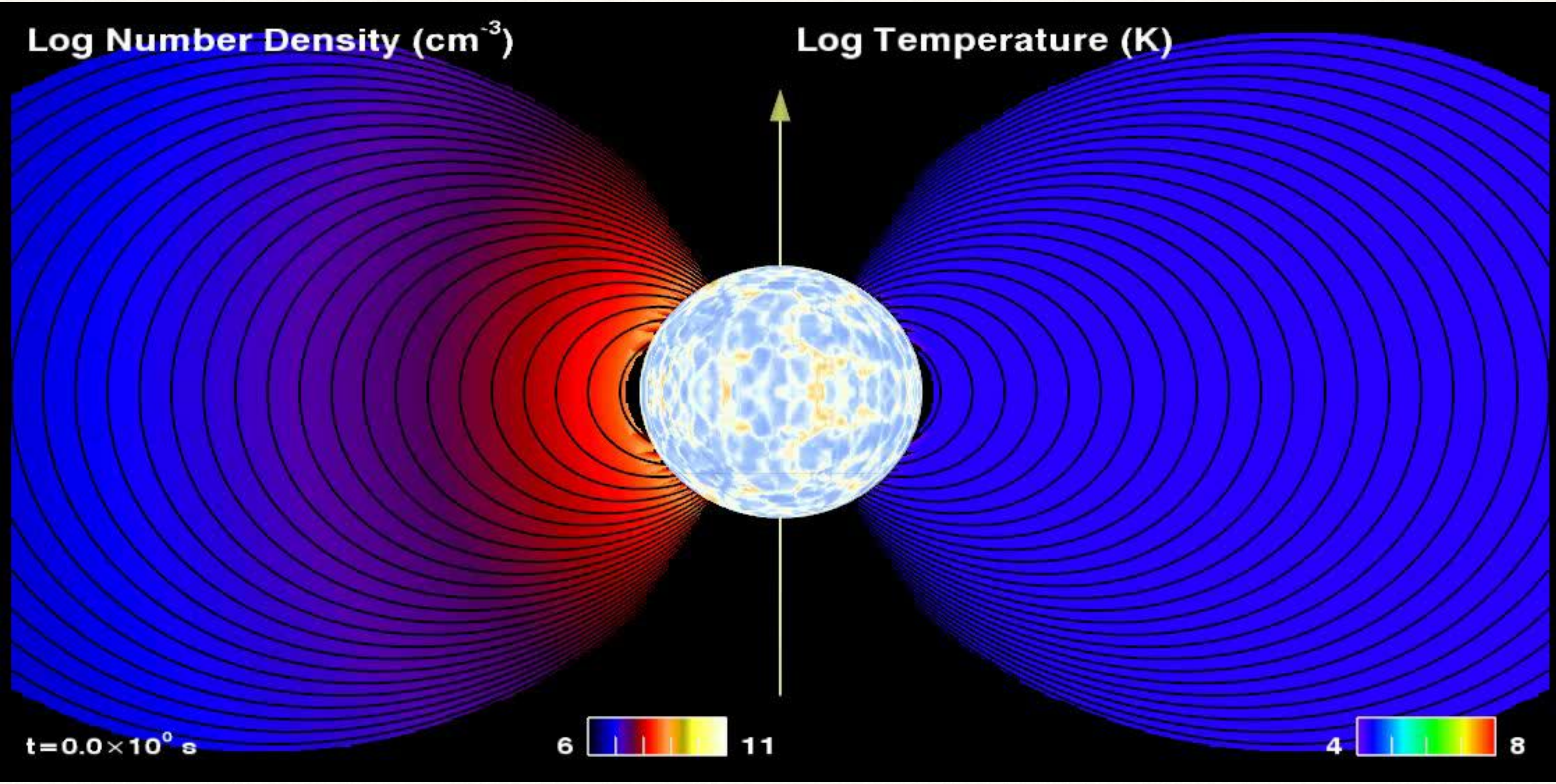

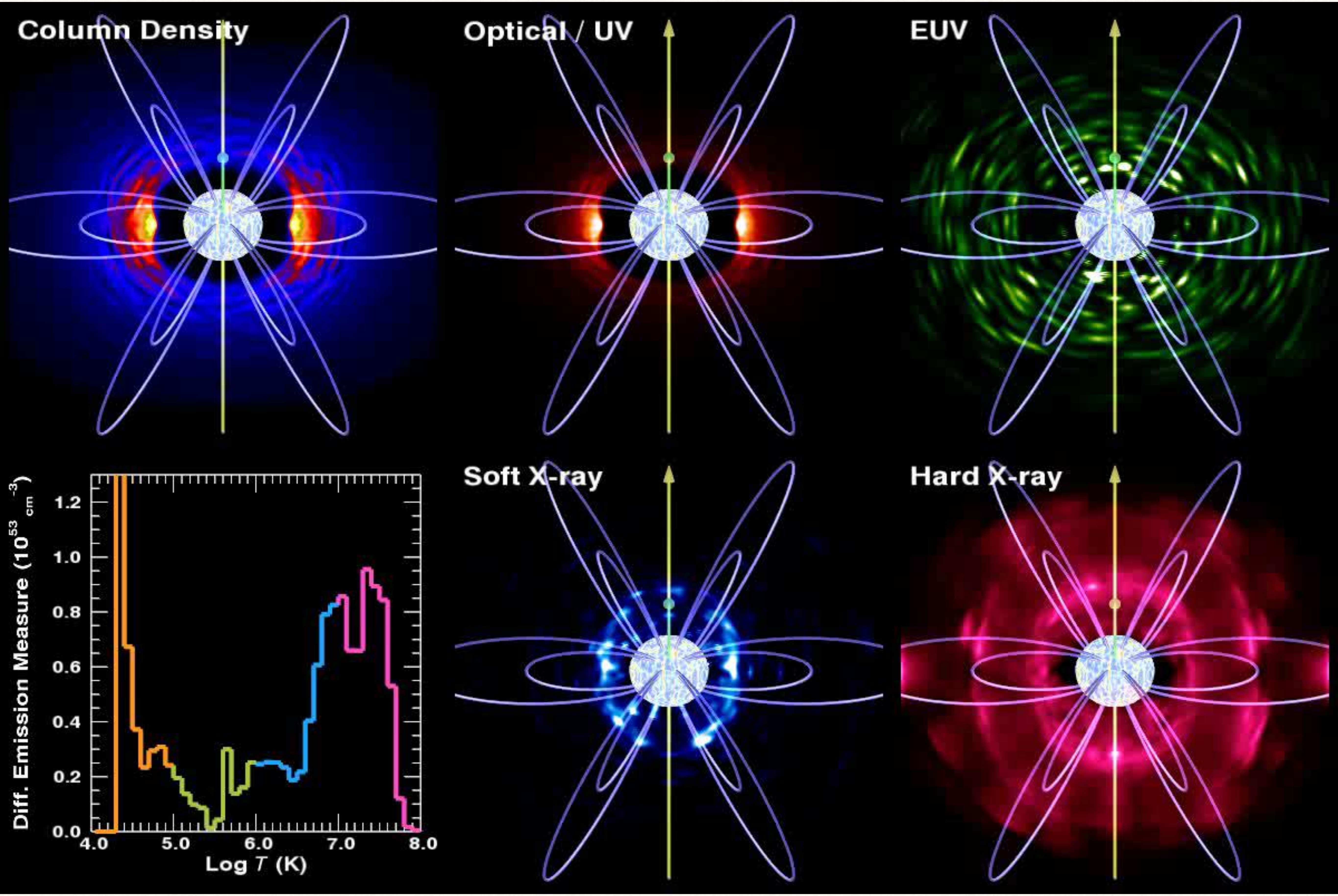

Column Density
Optical / UV
EUV
Soft X-ray
Hard X-ray
Diff. Emission Measure (10^{53} cm^{-3})
Log T (K)
0.0
0.2
0.4
0.6
0.8
1.0
1.2
4.0
5.0
6.0
7.0
8.0

Ultimately need 3D MHD

Iso-contour colored with radial V

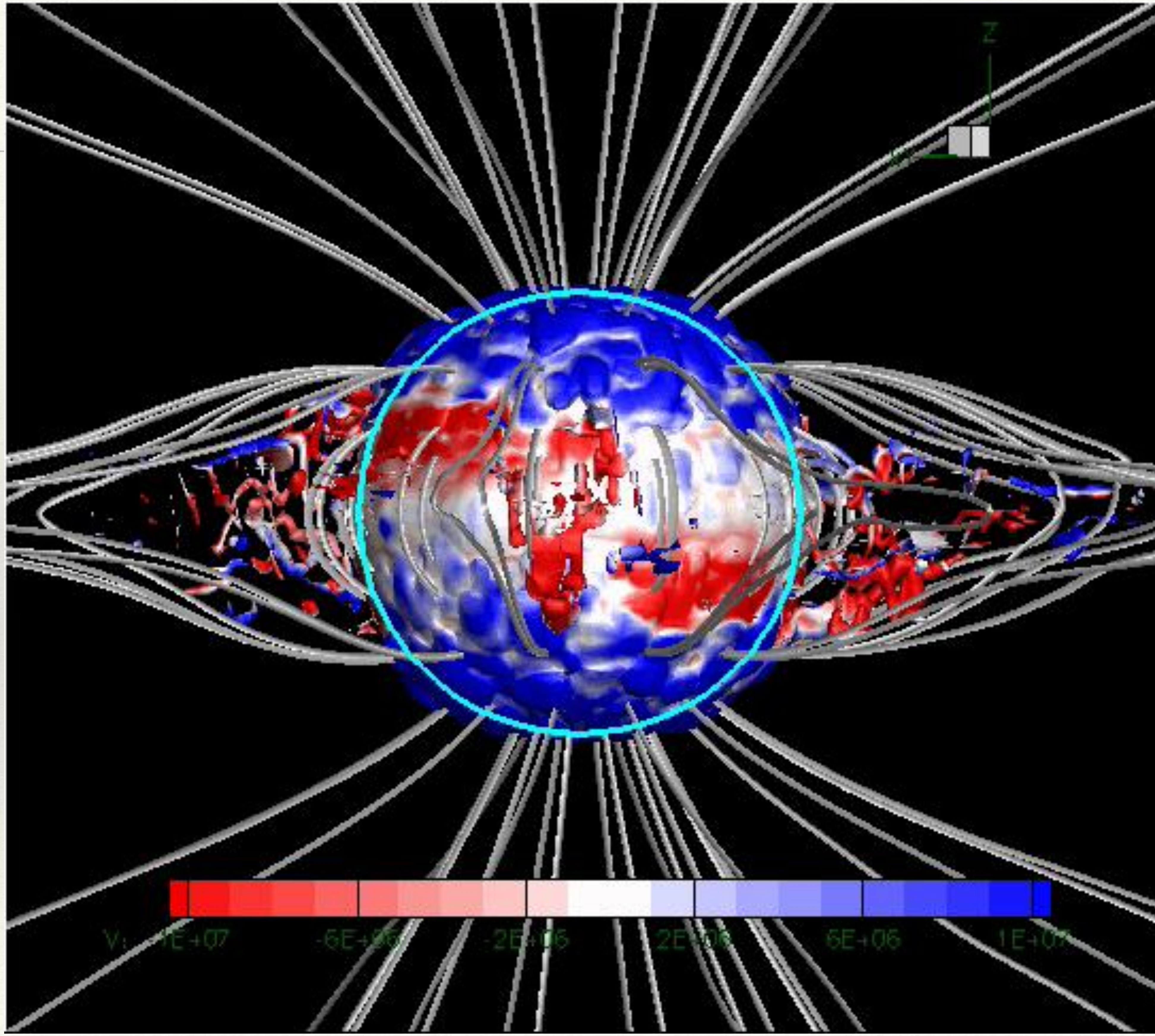

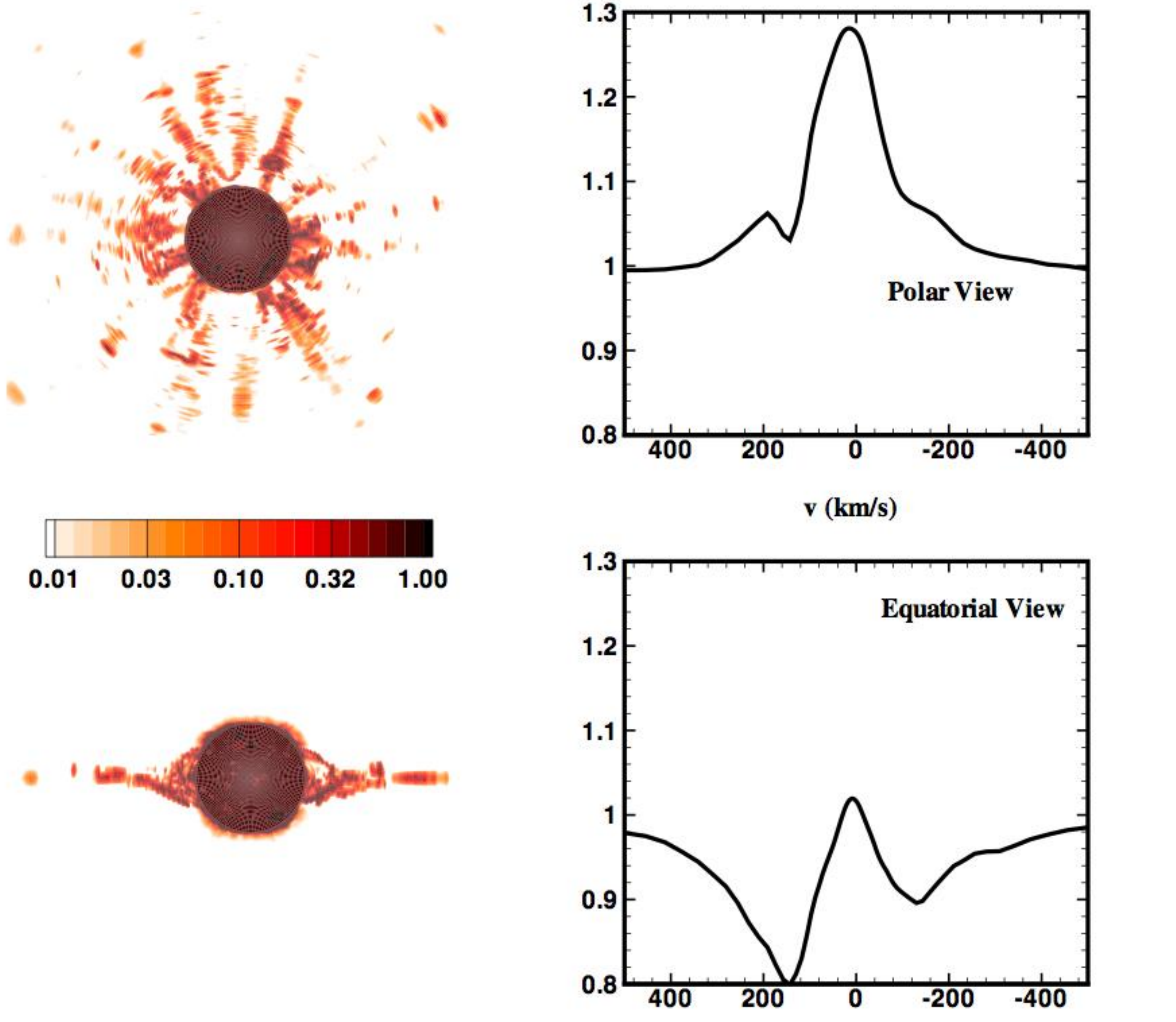

Figure 5. Synthetic Hα surface brightness maps (left panels) and flux profiles (right panels) for observer viewing angles above the equator (upper panels) and magnetic pole (lower panels), as calculated from a snapshot of the 3D MHD wind simulation taken at 1000 ksec after initialization.

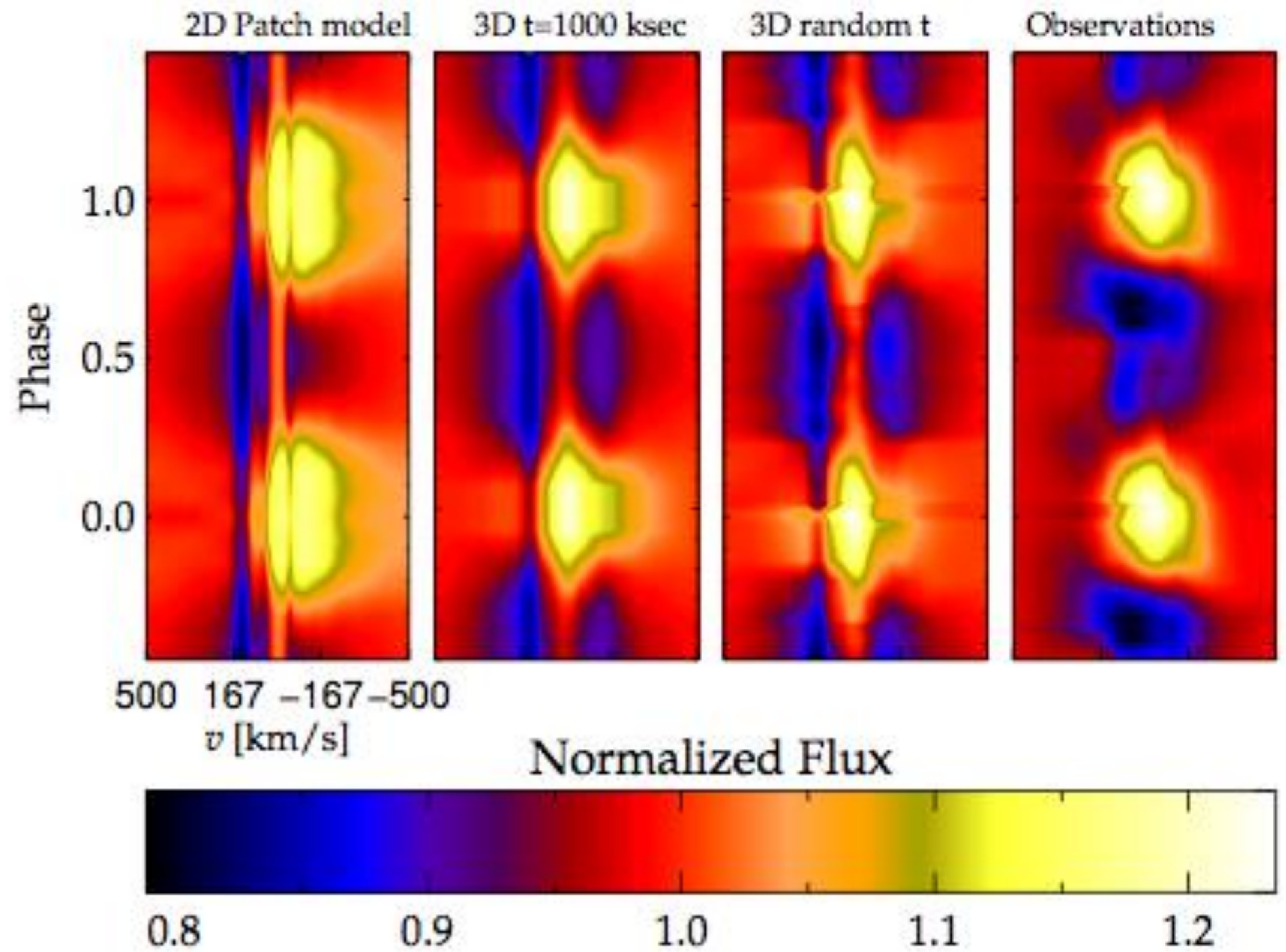

Figure 6. Observed and synthetic Hα dynamic spectra of θ^1 Ori C. Synthetic spectra calculated from patching together 2D model snapshots (panel 1), a single 3D model snapshot (panel 2), and from a random selection of 3D snapshots (panel 3). For consistency, 3D snapshots having random phases that coincide with the observations have been selected in the third panel.

ud-Doula et al. 2013

Oblique Dipole Challenging

$\beta = 45^o, \log(\eta_*) = 3.0$, W=0.7

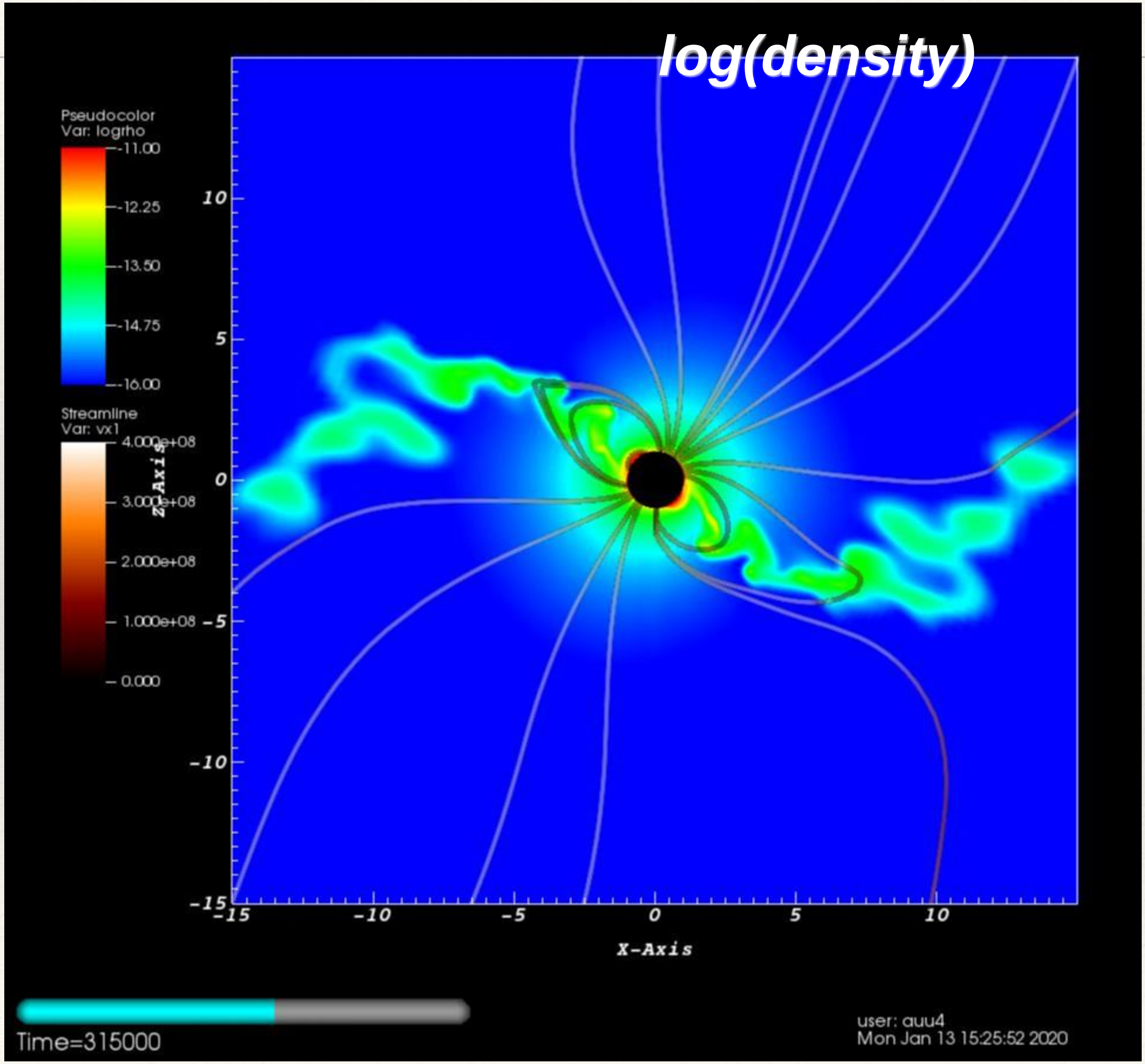

$\beta = 45^o, \log(\eta_*) = 3.0$, W=0.7

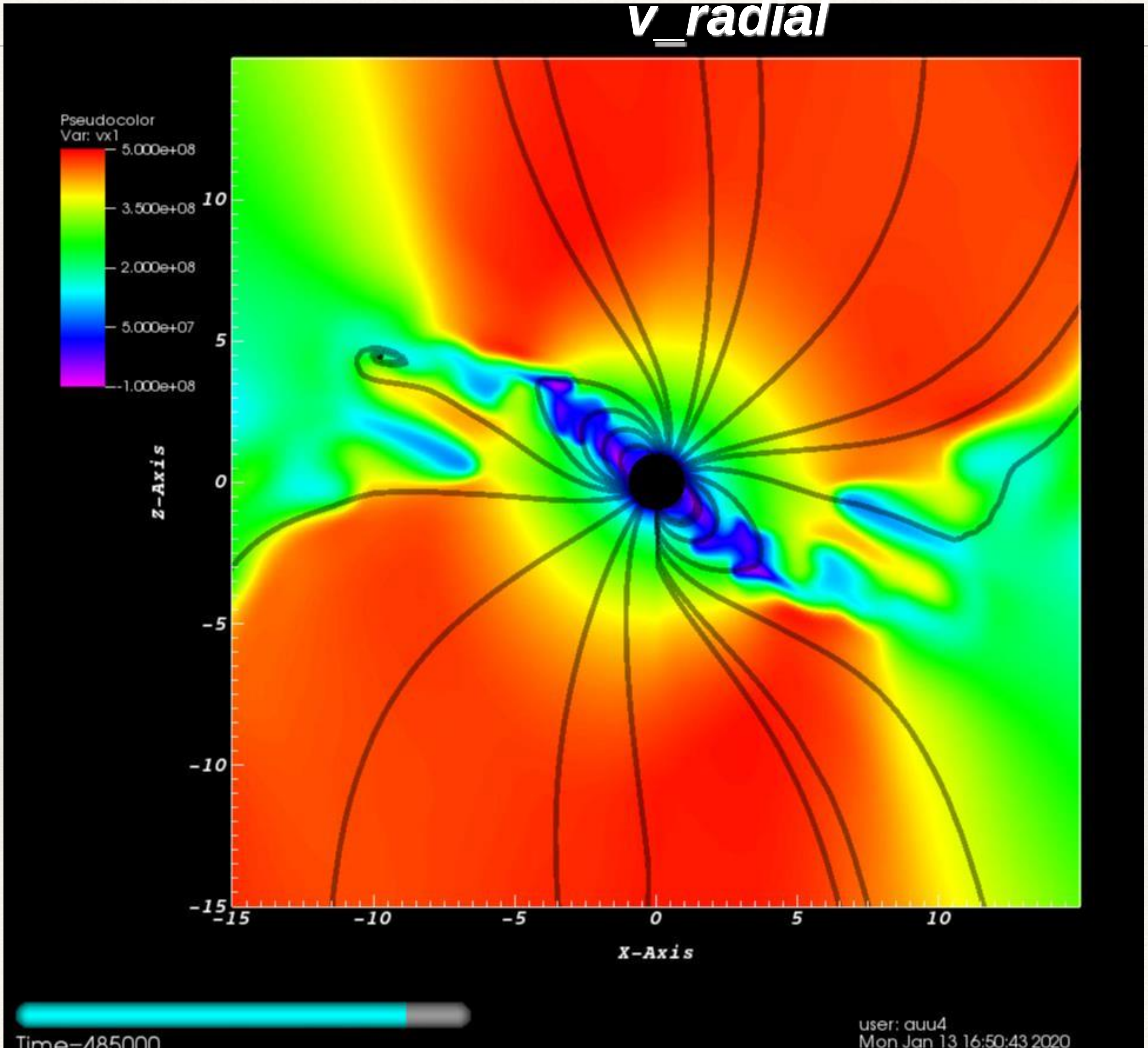

$\beta = 45^o$, $\mathrm{LOG}(\eta_*) = 3.0$, W=0.5

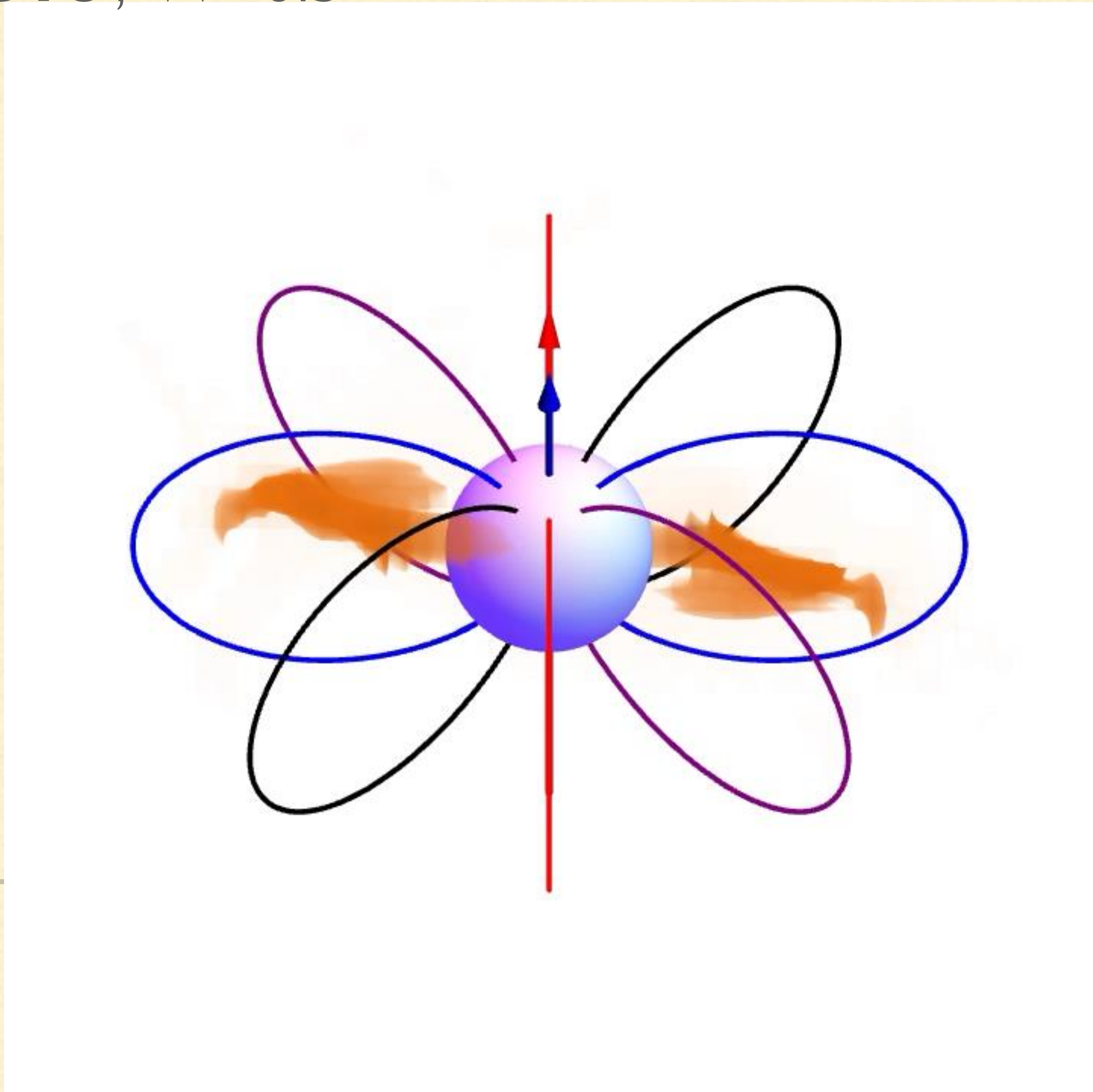

DENSITY DISTRIBUTION

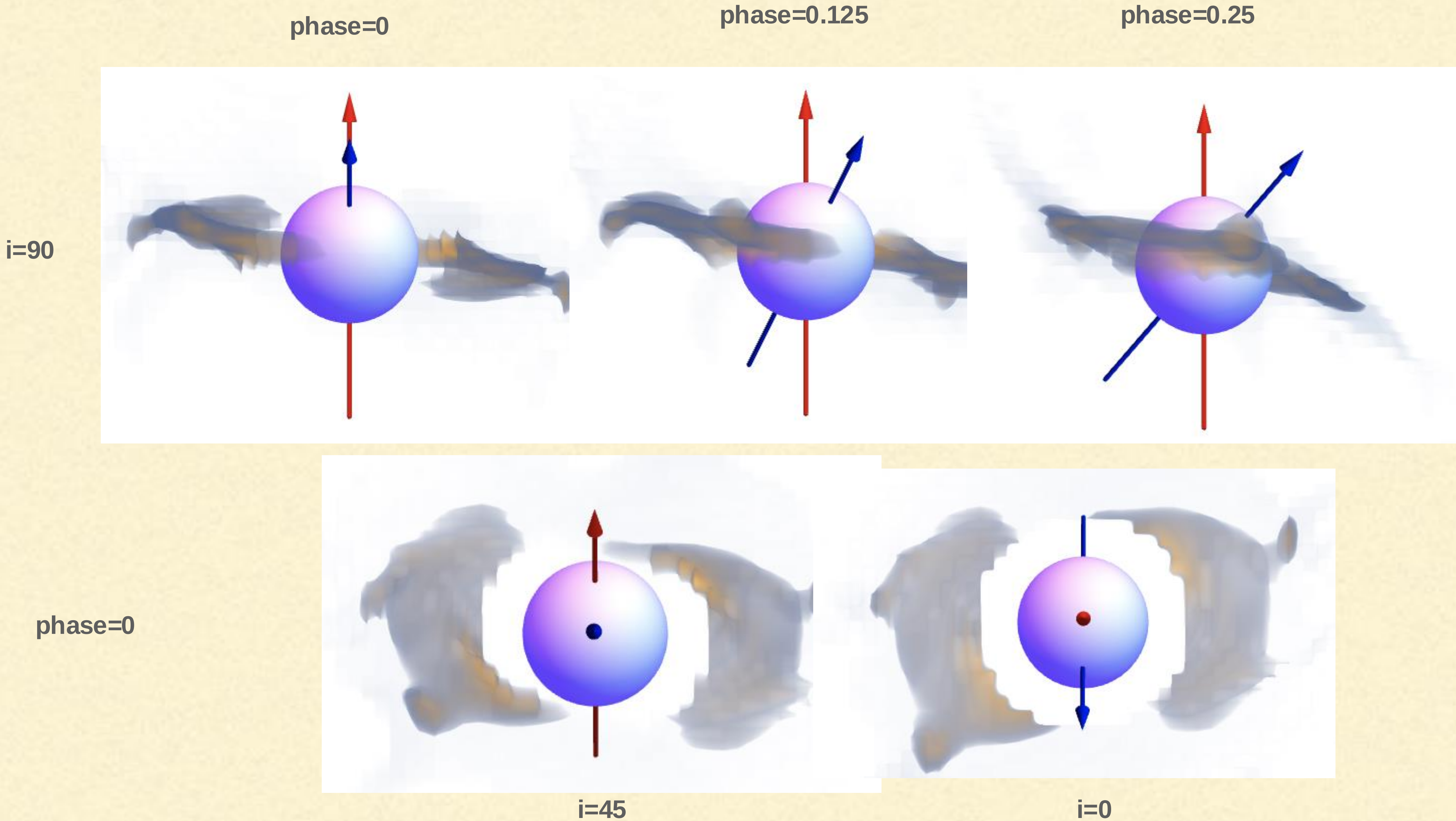

COMPARISON WITH RRM

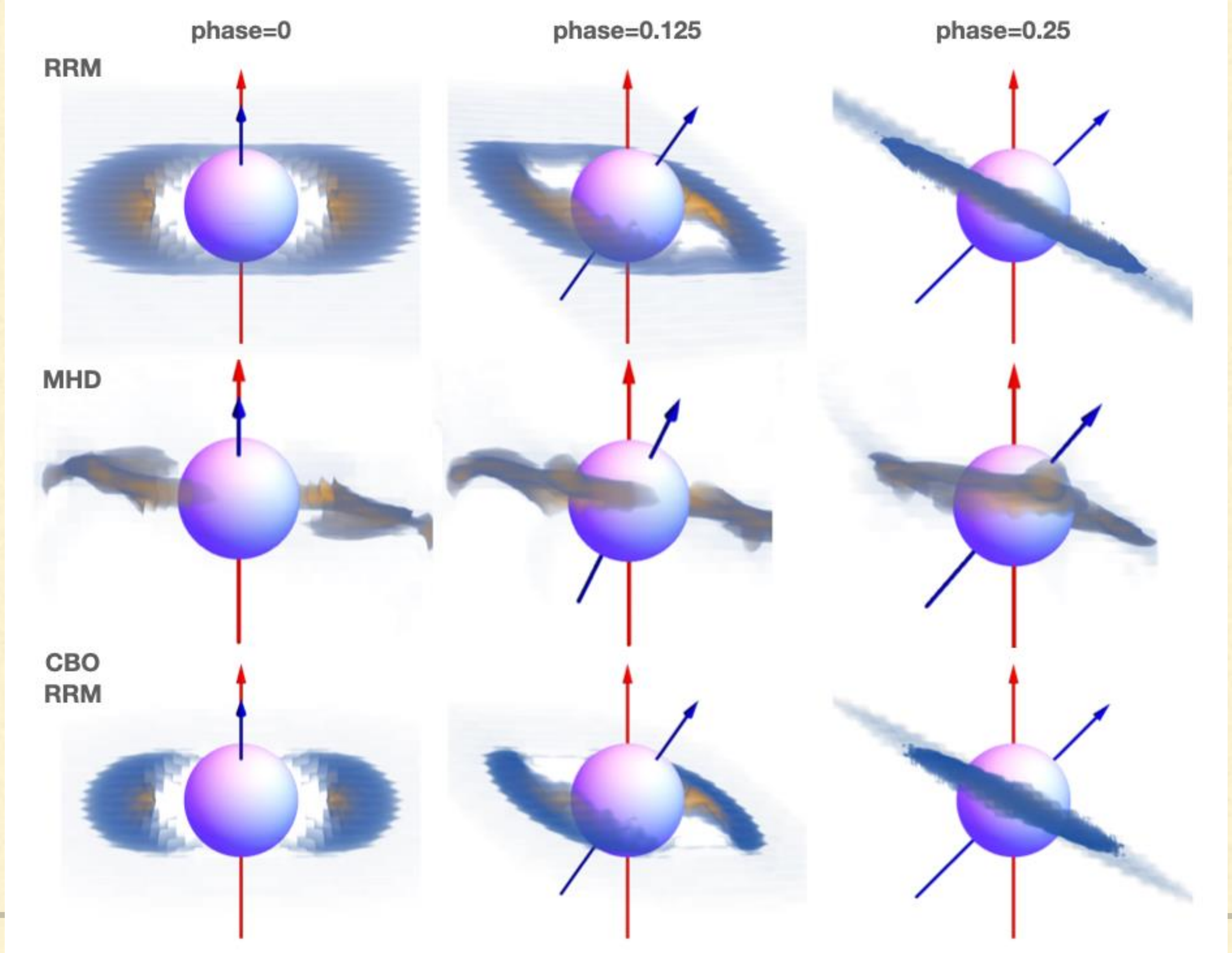

SYNTHESIZING HALPHA

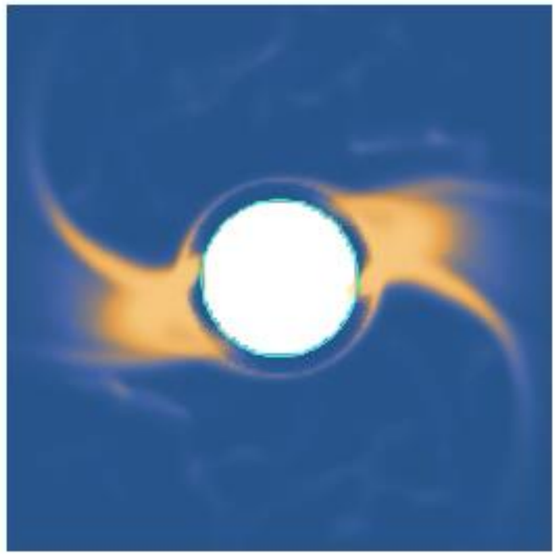

Halpha Line Profile

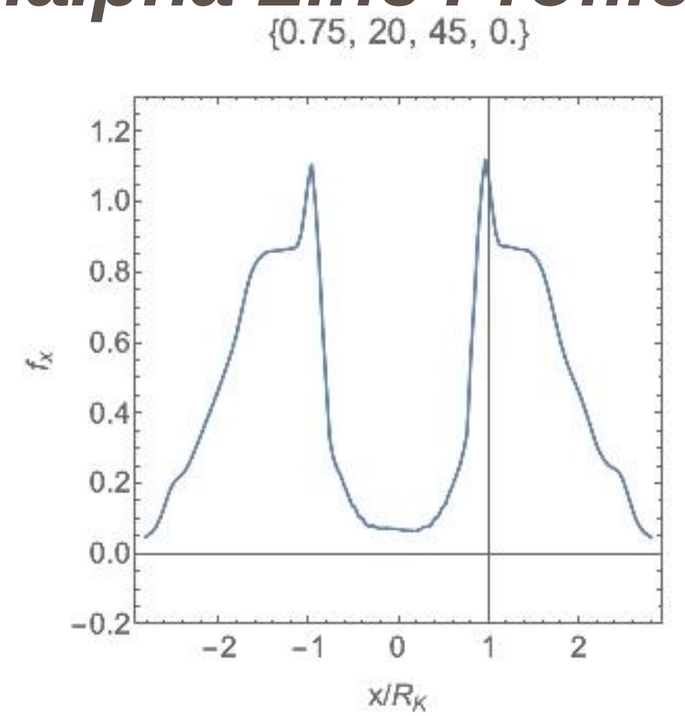

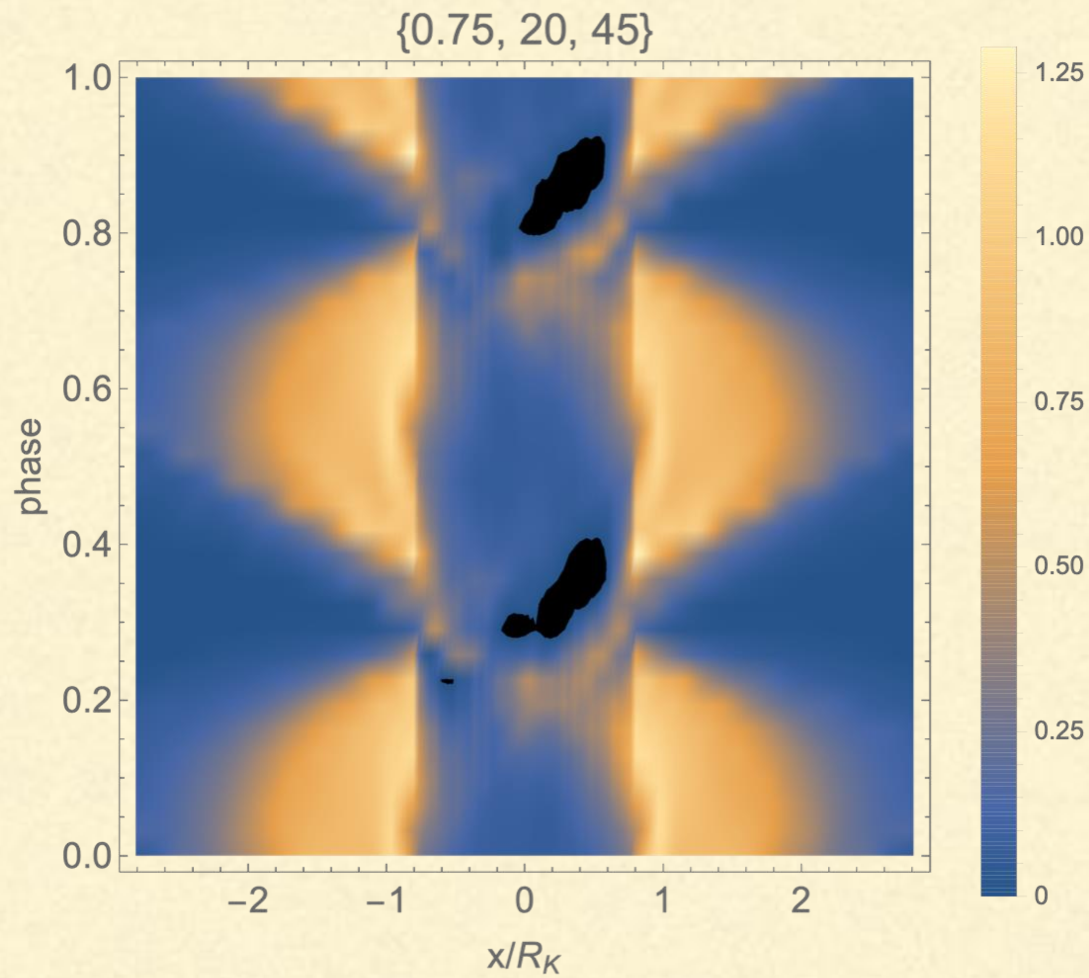

Dynamical Spectrum

ΗΑΛΠΗ
Α

RRM

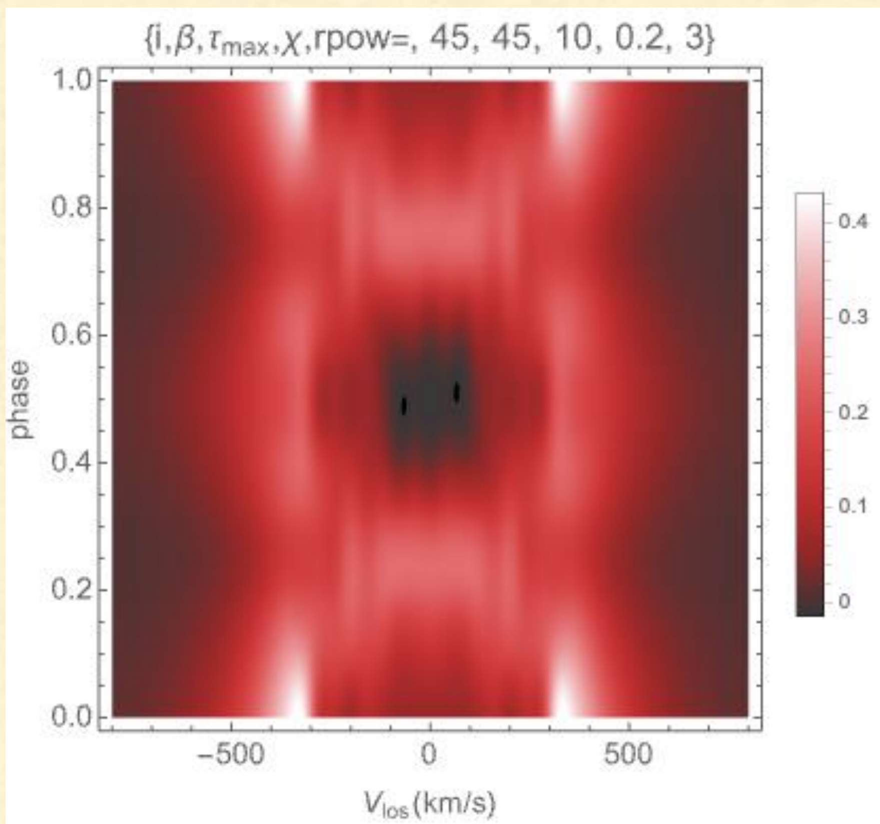

Rigid MHD

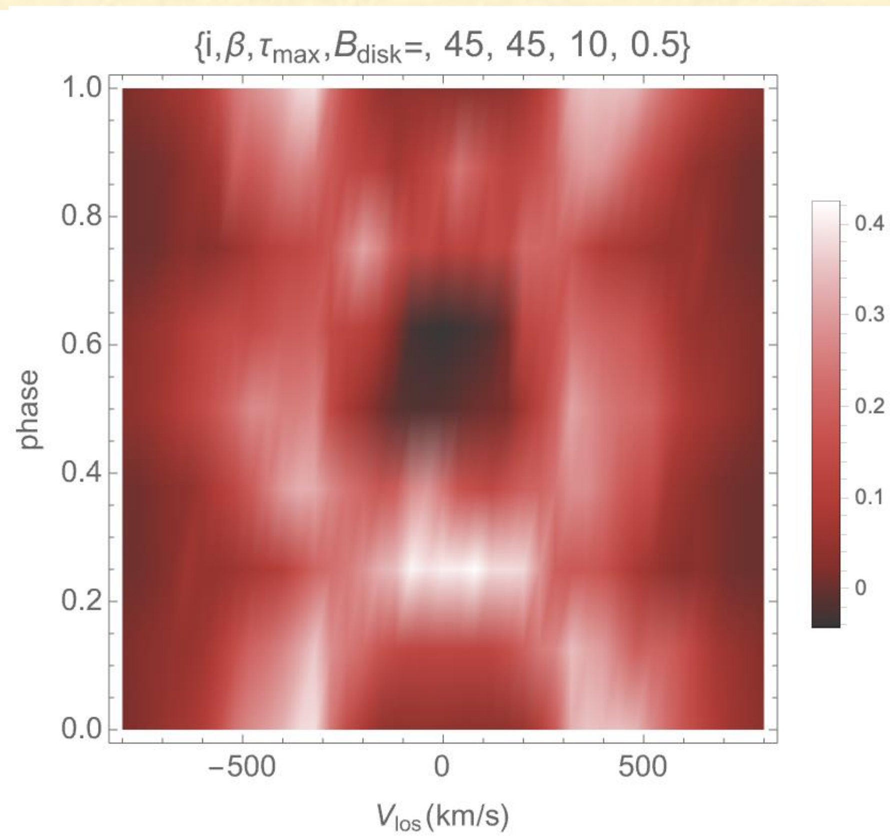

Full MHD

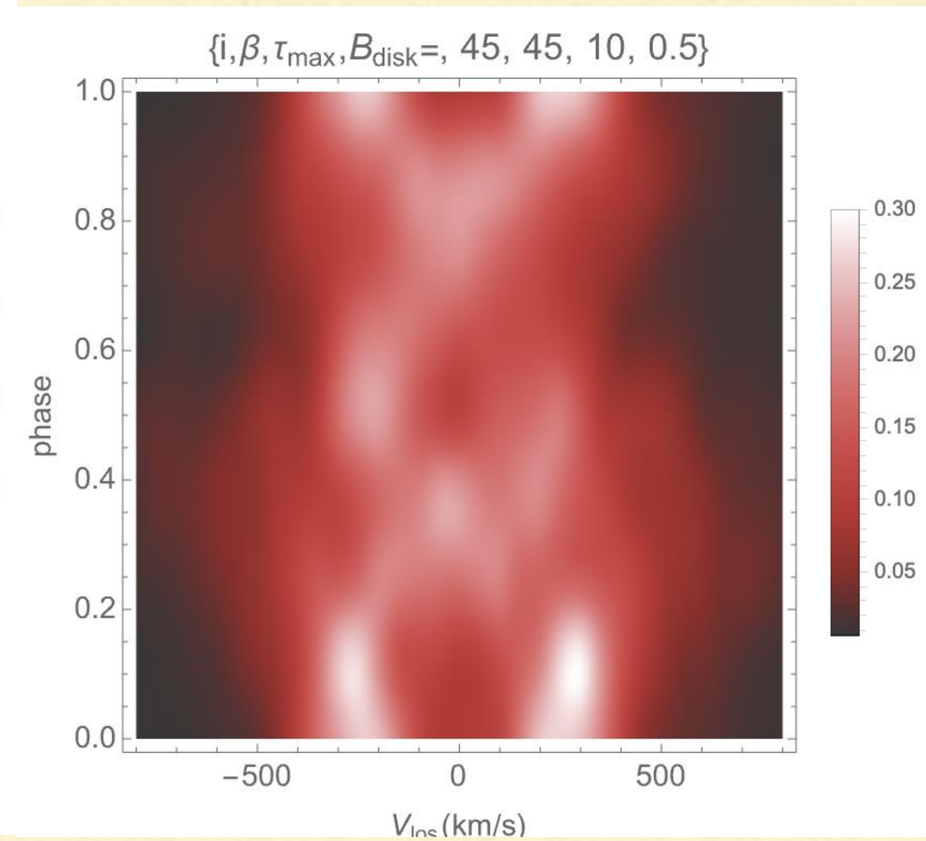

inclination 45deg

PHOTOMETRIC VARIATION

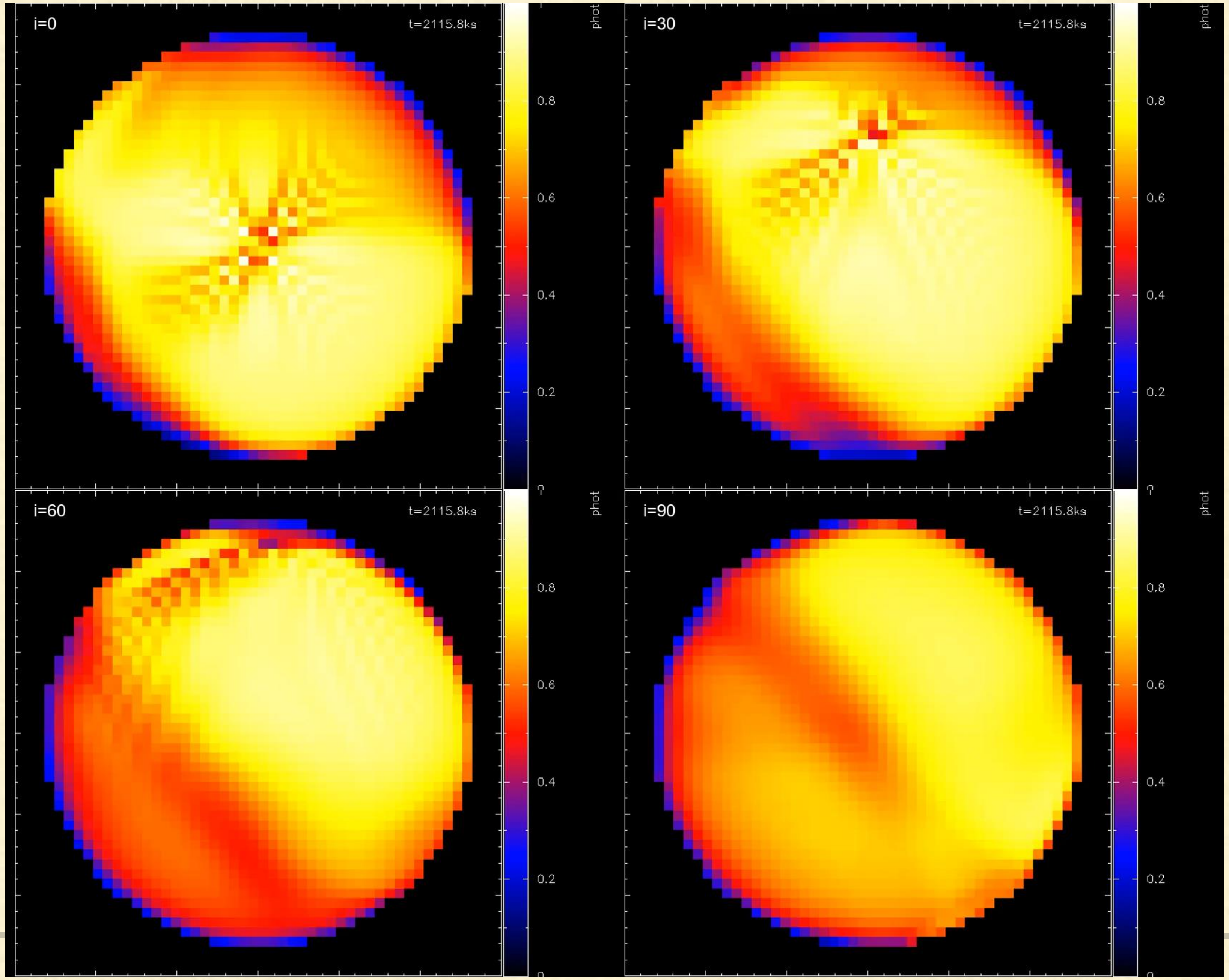

Conclusion

- 2D MHD of MCWS
  - slow rotating magnetic stars
  - can predict X-rays from magnetic stars
- Comparison with observations
  - Chandra & XMM
  - Optical photometry, spectroscopy, polarimetry
- 3D MHD of MCWS
  - 3D MHD for single stars can be done even for tilted dipole.
  - Basic disk topology is different from the one predicted by RRM model. In addition, there is significantly more variability in MHD models.
  - RRM assumes full rigid rotation; MHD suggests moderate breakdown due to rotational effects